![Royal Society Publishing logo — Informing the science of the future]

Flow Past a Circular Cylinder on a β -Plane
Author(s): D. L. Boyer and P. A. Davies
Source: *Philosophical Transactions of the Royal Society of London. Series A, Mathematical and Physical Sciences*, Vol. 306, No. 1496 (Oct. 15, 1982), pp. 533-556
Published by: The Royal Society
Stable URL: http://www.jstor.org/stable/37151
Accessed: 05/10/2008 09:54

FLOW PAST A CIRCULAR CYLINDER ON A β-PLANE

By D. L. BOYER† AND P. A. DAVIES‡

† *Department of Mechanical Engineering, University of Wyoming,*
Laramie, Wyoming 82071, U.S.A.

‡ *Department of Civil Engineering, University of Dundee, Dundee DD1 4HN, U.K.*

[Plates 1–10]

CONTENTS

With a view to obtaining a fuller understanding of the interactions between topography and large-scale geophysical flows, a series of laboratory investigations have been performed on the flow past a right circular cylinder in a rotating water channel. For large-scale flows on a spherical Earth the variation of the Coriolis parameter, $F = 2\Omega \sin \phi$, with latitude, ϕ, is commonly written (Pedlosky 1979) as $F = f + \beta_0 y$ where $f = 2\Omega \sin \phi_0$, $\beta_0 = 2\Omega \cos \phi_0 / R_E$, y is the distance to the north from the reference latitude ϕ_0, and R_E and $\Omega (= 7.29 \times 10^{-5} \text{s}^{-1})$ are the radius and rotation rate of the Earth respectively.

In this paper we shall discuss laboratory experiments in which the variation of F can be simulated. We shall refer to those studies in which $\beta = 0$ (i.e. the Coriolis parameter is uniform over the latitudinal extent of the region under investigation) as f-plane experiments. Models for which β_0 is non-zero will be referred to as β-plane experiments.

In the experiments the β-effect has been simulated by tilting the upper and lower surfaces of the channel so that the depth of the fluid varies in the cross-stream direction. Flow patterns have been obtained over a range of five independent non-dimensional parameters: Rossby and Ekman numbers, cylinder aspect ratio, β-parameter and flow direction ('eastward' or 'westward').

A dramatic difference in downstream behaviour is found between f-plane, β-plane westward and β-plane eastward flows. In particular, the β-plane eastward flows are characterized by bunching and pinching of streamlines in the wake region, the generation of damped stationary Rossby waves and downstream acceleration. Compared with f-plane flows the β-effect is shown to inhibit boundary layer separation from the cylinder for eastward flow and to enhance the separation for westward flow. Data are presented from all cases to show the asymmetry of the downstream flows and the transitions from fully attached to unsteady flows.

Under otherwise identical conditions the downstream extent of the separated-bubble region is much greater for β-plane westward flow than, in turn, for f-plane and

β-plane eastward flows. In addition, the data indicate that the size of the bubble increases with increasing Rossby number and decreases with increasing Ekman number and cylinder aspect ratio. For eastward flow the bubble size decreases with increasing β-parameter and for westward flow it increases with increasing β-parameter. Unsteady flows are investigated and instances of asymmetrical vortex shedding are presented.

1. INTRODUCTION

The flow of a homogeneous incompressible fluid past a right circular cylinder in a non-rotating frame of reference is regarded as a classical problem in fluid dynamics. The review article by Berger & Wille (1972), the discussion in the textbook by Batchelor (1970), and the recent experimental studies of Coutanceau & Bouard (1977) and Gerrard (1978) are good starting points for a study of the subject.

It is well known that the flow characteristics of this physical system depend on one dynamical dimensionless parameter, the Reynolds number, $Re = UR/\nu$, and, for confined flows past cylinders of finite length, the geometrical parameters defining the aspect ratio of the cylinder, R/H, and the ratio of the radius of the cylinder to the distance from the cylinder axis to the wall confining the fluid, R/L. Here U is the free-stream speed, R and H the cylinder radius and length respectively, ν the kinematic viscosity of the fluid, and $2L$ the dimension of the experimental apparatus measured normal to the free-stream velocity and the cylinder axis; see figure $1a$ with $\omega = 0$.

FIGURE 1. Schematic representation of the flow configuration used for
(a) f-plane and (b) β-plane studies.

The influence upon the flow character of varying the geometrical parameters R/H and R/L was investigated respectively by Nishioka & Sato (1974) and Coutanceau & Bouard (1977). It is of course true that other dimensionless parameters accounting for such factors as free-stream turbulence, roughness of the cylinder and the streamwise dimension of the experimental apparatus might also be important but these are not considered further in the present discussion.

The physical system in which the flow takes place in a frame of reference rotating uniformly about a vertical axis, with the cylinder axis also being vertical (see figure $1a$), has not received much attention. Because of the importance of background rotation on geophysical motions, such a system is of interest to meteorologists and physical oceanographers studying topographic effects on air streams and ocean currents.

For example, the international meteorological community is currently planning an important field experiment to study cyclogenesis in the lee of the Alps (Alpine experiment: Alpex); see GARP (1978). Jule G. Charney suggested, during the UNESCO Summer School in Venice in 1973, that vortex shedding resulting from flow separation in the lee of mountain ranges might be a mechanism for cyclogenesis. It is of course true that atmospheric phenomena such as cyclogenesis are far more complex than those represented by the physical system being considered in this paper. Nevertheless, it is expected that certain features of atmospheric (or oceanic) flow past large mountains or mountain ranges might exhibit some gross similarities to the flow past a cylinder as being considered here. This view has been advanced in a recent theoretical study by Merkine & Solan (1979).

The shedding of vortices by isolated mountain topography is an atmospheric phenomenon that has been recognized by meteorologists for many years (see Gjevik (1980) for a historical review) though visual verification by satellite photography has been made possible only recently. There are now numerous case studies of atmospheric vortex streets in the literature, all
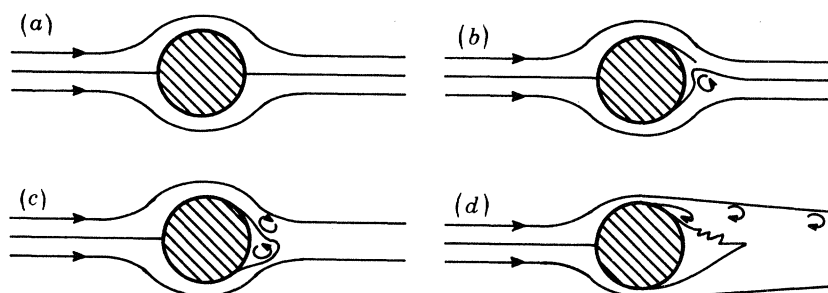
FIGURE 2. Schematic flow diagrams for f-plane flows illustrating (a) fully attached flow, (b) eddy formation, (c) steady asymmetric double eddies and (d) unsteady eddies. N.B. The sense of the background rotation is anticlockwise on this and all subsequent figures.

of them using data from satellite-observed cloud patterns (see Gjevik 1980). There are further geophysical motivations for this work: for example, an improved understanding of such a physical system in the laboratory, especially the character of the wake, could be of importance in the study of ocean currents past islands (see Hogg's (1980) review article on the general aspects of topography effects on ocean currents). The existence of stable eddy pairs downstream of Tobi island in the western Pacific has recently been discussed by Imberger & Johannes (1981).

We now return to the specific system depicted in figure 1 a where the upper and lower bounding surfaces are parallel and horizontal; we call this the f-plane configuration. A dimensional analysis leads to the conclusion that one more dynamical parameter must be considered than for non-rotating flows. In the study of rotating fluids it has become customary to introduce two new parameters: the Rossby number, $Ro = U/2\omega R$, and the Ekman number, $Ek = \nu/2\omega R^2$, where ω is the rotation rate of the system. Note that the Reynolds number (the ratio of Rossby to Ekman number) is thus not an independent parameter. In the following the Reynolds number will in general not be used explicitly, although it can always be calculated easily.

Background rotation has a major effect on the characteristics of the flow field past a cylinder, especially in the wake. One of us, Boyer (1970), developed a rotating water tunnel facility which could be used to investigate the system depicted in figure 1a. That study was addressed to producing a map of Rossby against Ekman number indicating the various flow patterns obtained for the range of parameters attainable from the apparatus.

To orient the reader to the β-plane studies (the principal thrust of the present investigation), the results of that f-plane study are briefly reviewed here. Figure 2 illustrates the series of flow patterns in the interior (i.e. outside boundary layers on the cylinder and channel surfaces) of the fluid that were observed as the free-stream velocity was varied from very low values to the largest values obtainable; i.e. with fixed Ekman number and increasing Rossby number.

At very low speeds and with $Ro \ll 1$, $Ek \ll 1$ the flow is essentially fully attached with the interior motion resembling potential flow. Recent theoretical f-plane studies by Walker & Stewartson (1972) and Merkine & Solan (1979) predict that the flow will be fully attached if

$$Ro \leqslant \frac{R}{H}\left(\frac{Ek}{2}\right)^{\frac{1}{2}}, \tag{1.1}$$

where it is noted that the Walker & Stewartson study refers to an analysis made by Buckmaster (1969) on a similar mathematical problem arising in the study of the viscous boundary layer on a cylinder with a strong applied radial magnetic field. One other theoretical prediction referred to by Walker & Stewartson is that for the Rossby number range given by

$$\frac{1}{2}\frac{R}{H}\left(\frac{Ek}{2}\right)^{\frac{1}{2}} \leqslant Ro \leqslant \frac{R}{H}\left(\frac{Ek}{2}\right)^{\frac{1}{2}} \tag{1.2}$$

the flow separates but has no reverse flow and that, in addition, the motion is inherently unstable. The prediction (1.2) was obtained by Leibovich (1967) in the analysis of the magnetohydrodynamic boundary layer problem referred to and clearly is in conflict with (1.1). We shall return to the experimental considerations of these theoretical predictions later; it is noted, however, that the present experiments support the fully attached criterion given by (1.1).

Boyer (1970) found that as the free-stream speed is increased to values for which separation begins to take place the wake flow develops a distinct asymmetry between the right and left sides (facing downstream). For example, at sufficiently large free-stream speeds a standing eddy is found downstream of the cylinder as shown in figure 2b. At larger velocities the wake region develops an asymmetric double-eddy system with the eddy on the right being attached to the cylinder and that on the left occurring away from the cylinder surface (figure 2c). At still larger velocities both eddies begin to develop an unsteadiness and at critical values of the free-stream speed the left-hand eddy sheds periodically but the right-hand one, although unsteady, remains attached (figure 2d). At still larger velocities eddies shed alternately from either side of the cylinder.

For uniformly rotating systems such as those being considered it is possible to simulate the β-effect by tilting the upper and lower surfaces of the fluid container from north to south, with the 'thin' portion toward the north (figure 1b) (see Greenspan 1968; Vaziri & Boyer 1977). We refer to the system in figure 1b as the β-plane configuration.

In considering flow past a cylinder on a β-plane we must thus introduce an additional dimensionless parameter, β, which, following Merkine (1980), we take as

$$\beta = \beta_0 R^2 / U.$$

As noted in the next section, β can be simulated in the laboratory by tilting both the upper and lower surfaces of the channel at an angle α to the horizontal (see figure 1b) such that

$$\beta = \alpha \frac{R}{H}\frac{1}{Ro}.$$

We shall take this as the β-parameter in the discussion that follows. In mid-latitudes $\beta_0 \approx 1.6 \times 10^{-13}\,\mathrm{cm^{-1}\,s^{-1}}$. For an ocean current of $10\,\mathrm{cm/s}$ and for $R = 100\,\mathrm{km}$, for example, $\beta \approx 1.6$. We shall thus be interested in laboratory experiments in which β is of order unity.

In a recent theoretical study, Merkine (1980) predicts that the β-effect inhibits boundary layer separation for prograde (eastward) flows but exerts no influence on the boundary layer structure for retrograde (westward) flows. Unfortunately, that theory requires the parameter restriction

$$Ek^{\frac{1}{2}} \ll RoH/R, \tag{1.3}$$

which cannot strictly be met in the experiments to be discussed. Nevertheless, as will be noted later, the β-effect does tend to inhibit separation for eastward flow in the experiments so that the Merkine analysis is of some interest here.

Theoretical and experimental studies of flow past a cylinder on a β-plane were made by White (1971) who considered the zonal flow past an island. The theoretical work, in which viscous effects were neglected, indicated that retrograde-flow streamlines departed little from potential-flow streamlines while in prograde flow Rossby waves could be generated downstream of the island. White also presented some experimental evidence for his theoretical calculations, but the experiments did not examine systematically the wake characteristics as a function of the system parameters. Long (1952) investigated the motion of a circular obstacle extending between the upper and lower surfaces of a rotating spherical shell. No detailed data were presented on the resulting flow fields and their variation with the system parameters.

Finally, predominantly qualitative experiments on flow past isolated truncated topographies on a β-plane (generally with the goal of investigating Taylor columns) were made by McCartney (1975), Vaziri (1977) and Takematsu & Kita (1978).[†] For a more detailed analysis of the various laboratory experiments concerning topographic effects in rotating flows the reader is referred to a review article coauthored by one of the present authors, Baines & Davies (1980).

In summary we note that only a limited theoretical effort has been made on the physical system in question and that the only systematic experimental programme was conducted by one of the present authors (Boyer 1970). However, this experimental study was limited to characterizing the resulting flow fields on a Rossby against Ekman number map; i.e. no quantitative data for the characteristics of the wake were obtained.

We also note that wake flows from topographic features on both f- and β-planes have potentially important applications in meteorology and oceanography and that little detailed, systematic, laboratory experimental work is reported in the literature concerning such systems. A major motivation for such a study was the need to provide laboratory data useful for theoretical studies of the problem. Accordingly, we designed an experimental programme to investigate the characteristics of flow past a cylinder on a β-plane (and an f-plane, i.e. $\beta = 0$) for as wide a range of system parameters as practicable. The main objectives of the studies were as follows:

(i) to delineate the general character of the flow external to the boundary layers on the channel and cylinder surfaces;

(ii) to quantify, to the extent possible, the size of the eddy systems downstream of the cylinder;

(iii) to determine the separation angles on both the right and left sides of the cylinder (facing downstream).

Because of the large number of dimensionless parameters that characterize the system, it is

† A quantitative study of this problem has recently been completed by the present authors and a report is currently being prepared for publication.

difficult to devise a detailed experimental design having a tractable number of runs. The following six parameters enter: Ro, Ek, β, R/H, flow direction (eastward or westward) and R/L. The design decided upon was addressed to investigating the system for variations in all of these except R/L; L and H had fixed values and hence R/H and R/L were varied at the same time. Thus, any flow-pattern changes due to variations in these parameters had to be attributed to a variation in both; i.e. individual dependence could not be resolved.

In § 2 we describe the experimental apparatus and techniques. In § 3 the results of the experimental programme are presented, with concluding remarks being made in § 4.

2. EXPERIMENTAL APPARATUS AND TECHNIQUES
2.1. Apparatus

A schematic representation of the experimental apparatus is shown in figure 3. The essential components of the arrangement were (a) a water channel, C, having specially designed inlet and outlet baffles, B and B′ respectively; (b) a pumping system, P, to produce a given flow through the channel; (c) an appropriate flow visualization facility, FV; and (d) a solid obstacle fixed in
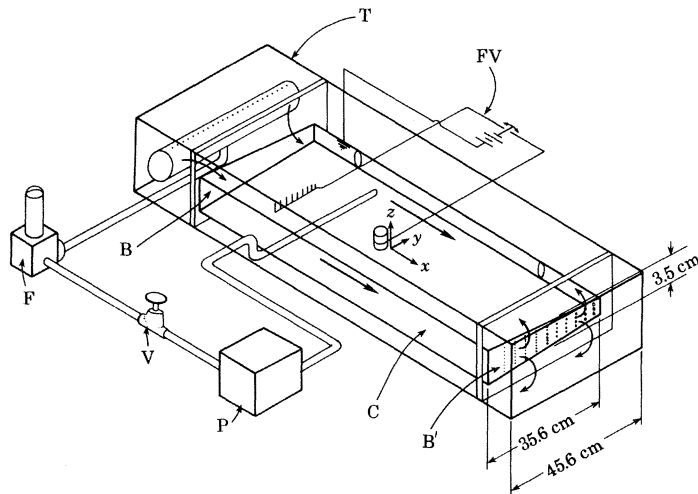

FIGURE 3. Schematic representation of the laboratory apparatus.
(See text for explanation of lettering.)

position in the channel and extending throughout the full depth of the working fluid. The whole apparatus was mounted on a large turntable, the rotation rate of which could be varied continuously between 5 and 25 revolutions per minute in either a clockwise or an anticlockwise sense. A camera mounted on the turntable recorded horizontal flow patterns in the working section of the channel.

Details of the construction of the water channel have been presented previously (Vaziri 1971; Vaziri & Boyer, 1971). In the present experiments, the top and bottom bounding-surfaces of the channel were not, in general, parallel to each other. To model the β-effect, the channel was constructed with each of the surfaces inclined to the horizontal by a small angle, α (see figure 1b).

Five different values of α (0.00, 0.0134, 0.0268, 0.0402 and 0.0536) were used in the experiments. The working channel, which had a mean depth of 3.45 cm, a width of 35.6 cm, and a length of 129.5 cm, was supported at each end by a recessed baffle arrangement, B, B', within a large rectangular tank, T, filled with water. The seats between the working channel and the baffles were sealed with rubber gaskets to ensure that all of the fluid pumped through the system passed through the working channel via the inlet and outlet baffles. The flow through the system could be varied and monitored by means of a valve, V, and flowmeter, F, in series with the pump. The temperature of the fluid was monitored throughout a given experimental run. The tank, the working channel and the baffles were made from Plexiglass to allow visual observation of the flow.

The working section of the channel was illuminated from a light source mounted on the rotating table through a slit typically 5–10 mm wide and extending along the full length of the working section. The vertical positions of the slit and light source were adjustable so that flow details at various levels in the channel could be isolated. Most data were collected with the slit in the mid-depth position.

Several sets of baffles were used in the experiments to ensure that the undisturbed flow in the channel was uniform over a wide parameter range. The baffles consisted of plates of Plexiglass having an array of holes of varying size (see figure 3) and were modelled on those used earlier for this type of channel (Vaziri & Boyer 1971). The importance of inlet and outlet conditions in rotating channel flows has been emphasized elsewhere (Vaziri 1971; Hsueh & Legeckis 1973). With the arrangement chosen, the size and distribution of holes in the baffles can be chosen to eliminate cross-channel shear in the flow and to ensure that the basic flow direction coincides approximately with the long axis of the tank. Nevertheless, we note that each set of baffles is strictly appropriate to a single pumping speed–rotation rate combination. Since a range of these parameters were scanned during a typical series of runs some shear in the cross-channel direction had to be tolerated. This north–south shear could vary in sign, with the ratio of the maximum axial velocity difference to the mean free-stream velocity rarely exceeding 0.10. At this level, the vorticity associated with the cross-stream shear is negligible compared with both the inertial vorticity U/R and the background vorticity 2Ω. The effects of the presence of such a shear upon the flow can therefore be neglected.

Each of the cylindrical solid obstacles used in the experiments extended throughout the full depth of the working channel. For all investigations the plane surfaces of the cylinders were machined carefully to match the inclined top and bottom surfaces. Four different cylinders (radii 3.81, 2.54, 1.27 and 0.64 cm) were used in the investigation, each having the same mean height of 3.49 cm.

2.2. *Flow visualization*

The method of flow visualization used was an electrolytic precipitation technique developed by Honji *et al.* (1980) (see also Taneda *et al.* 1974, 1977; Honji & Ishi-i 1976). The method is based upon the observation that if a small potential difference (a few volts) is applied between a solder cathode and, say, a brass anode in an electrically conducting liquid, a white colloidal cloud is released from the solder. The technique was adapted to the present study by arranging a series of vertical solder wires upstream of the obstacle at regular but non-uniform intervals across the channel. The wires, though sufficiently rigid to withstand distortion by the moving fluid, produced negligible disturbance to the basic flow. Solder was also inserted into a groove machined around

the circumference of the obstacle at mid-height, so that tracer material could be introduced into the boundary layer on the obstacle. To avoid premature separation of the boundary layer induced by spurious roughness elements, care was taken to ensure that the solder ribbon was flush with the cylinder surface. A potential difference was applied between the two sets of solder probes and a large brass electrode placed on the floor of the outer tank. The electrical connections were made such that the two sets could be switched on and off separately. The bottom surface of the working section of the channel was painted black to enhance the contrast between the background and the white tracer released from the solder.

Difficulties are encountered with this method unless the electrical conductivity of the working fluid is carefully controlled. Tap water can be used successfully, though in the experiments described here distilled water was used to which a modest amount of common salt and a small amount (a few grams) of sodium carbonate was added. The optimum amount of salt required to avoid either too high conductivity (and resulting polarization bubbles) or too low conductivity (no tracer) was established by trial and error. For our apparatus of capacity $0.08\,\text{m}^3$ approximately one cup full of salt was satisfactory. Similarly, the voltage applied to the electrodes needs to be adjusted carefully to give sufficient tracer for effective observation and photography, while avoiding the emission of polarization bubbles. Because the surface of the solder degrades with time through the action of electrolysis, the probes required periodic replacement.

The tracer produced by the above technique is approximately neutrally buoyant. The velocities of the undisturbed flows were sufficiently high that the particles in the tracer did not settle out of the fluid within the main part of the working section. Within the wake region, however, flow velocities were typically not high enough to sweep away all of the dye generated on the boundary of the cylinder. As a result, in certain parts of the wake region tracer particles were observed to drop out of the colloidal cloud into the Ekman layer on the bottom surface of the channel. This effect is shown in some of the photographs presented in this paper. It should also be noted that air bubbles trapped between the working channel and the tank, are occasionally visible on the photographs; because they were outside the working channel, they had no effect upon the flow.

2.3. *Experimental procedure*

Each experimental run was conducted with a given cylinder, a given slope, α, and a given baffle set appropriate to the parameter range under investigation. All solder probes for the flow visualization were checked for adequacy before the start of the run.

The parameter values were varied systematically to obtain, as far as possible, a uniform grid in dimensionless parameter space; for example all parameters except one (e.g. Ro) were fixed and then that parameter was varied. Sufficient time was left between sets of observations to allow the flow to spin up to the steady state (or periodic unsteady régime). The temperature of the water was recorded throughout the run. For a particular combination of rotation rate, ω, and mean flow velocity, U, several observations were made. Firstly, a sequence of photographs was taken of the upstream flow to determine the shear (if any) in the undisturbed flow. Secondly, the overall flow pattern past the obstacle, as revealed by the continuous emission of tracer from the upstream probe array, was recorded, and, finally, a series of photographs was taken of the wake region of the flow with dye being released only from the solder ribbon on the obstacle. The last sequence indicated not only some of the details of the boundary layer separation but also the structure and extent of the downstream eddying.

3. EXPERIMENTAL RESULTS

Figure 4 depicts the Rossby and Ekman number and cylinder aspect ratio ranges examined for both the f- and β-planes. It is noted that the range of β investigated is $0 \leqslant \beta \leqslant 5$ and that for each β-value eastward and westward flows were studied. In the f-plane photographs given subsequently the flow is from left to right (i.e. 'eastward') and the rotation is anticlockwise. The same flow patterns would, of course, be obtained for 'westward' flow because for the f-plane there is no dynamical differentiation between 'east' and 'west'.

For experimental convenience westward flows are obtained by pumping the fluid 'eastward' and reversing the rotation of the table to clockwise. By examining the governing equations of motion in the flow channel, westward motion for Northern Hemisphere or anticlockwise rotation is then obtained by reversing the photographs by the transformation $x \rightarrow -x$, (see figure 1b). All of the westward flows were obtained in this way.
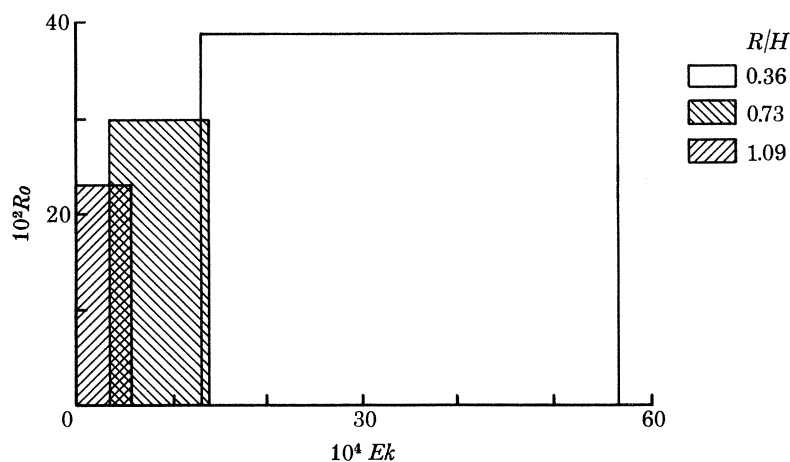

FIGURE 4. Domain diagram illustrating the ranges of Ro, Ek and R/H investigated in the experiments.

3.1. General observations

In this section we describe the principal qualitative observations made during the course of the experimental programme. Figures 5a–c (plate 1) show examples of the streamline patterns obtained for steady flow on an f-plane, and eastward and westward flow on a β-plane respectively. For all of the experimental photographs north will be towards the top, east to the right and so on. In these experiments the tracer is released along a series of vertical solder wires upstream of the cylinder. Since the flow is steady the streak lines represent streamlines of the flow. These photographs typify all experiments conducted for parameter combinations for which the flow is steady.

For the f-plane and β-plane westward flows, one apparent aspect of the flow patterns is that, when the flow is essentially fully attached, the interior flow away from the cylinder walls approximates potential flow past a cylinder in a non-rotating frame of reference. As the extent of the separated region increases (with increasing Rossby number, for example) the interior flow adjusts in a manner not dissimilar to that observed in the non-rotating case: i.e. the flow away from the eddies moves smoothly past the cylinder and the associated downstream bubble enclosing the eddies. For these flows the separation between adjacent streamlines, and the lateral streamline location far downstream of the cylinder, approximate those occurring in the free stream.

For the β-plane eastward case, the flow accelerates as it moves past the cylinder, with the wake region having a larger characteristic streamwise speed than the free stream: note the 'bunching' of the streamlines in the wake. This 'wake jetting' is common to all eastward flows investigated. The characteristic speed in the wake jet depends in a complex way on Ro, Ek and R/H. A quantitative estimate of this jetting effect can be made by comparing the separation of dye tracer lines such as that on figure 5b. Wake-jet speeds obtained in this way typically range from 1.3 to 2.0 times the free-stream velocity for the range of parameters considered in the present experiments. Note that for the example in figure 5b the wake-jet velocity is approximately twice that of the free stream.

Some eastward flows, in addition to being characterized by a convergence of streamlines in the wake, are accompanied by a 'pinching' in the downstream flow, i.e. a turning point in the flow exists downstream of the cylinder where streamlines initially having a northward component (right side, facing downstream) are diverted southward, and vice versa. In such cases the turning point (arrow in figure 6a, plate 2) is always located further downstream on the right-hand side (facing downstream), than on the left-hand side (see figure 5b as well as figures 6a–f).

The degree to which both pinching and downstream acceleration occur depends in a complicated manner upon the values of Ro, Ek, R/H, but the phenomena themselves are common to all eastward flows. Indeed, these eastward-flow characteristics are further illustrated in figure 6 for an extensive range of Ro, Ek, and β. The structure of the eastward flows suggests the presence of a damped, topographically induced, stationary Rossby wave downstream of the cylinder. Inviscid shallow water theory predicts that the wavelength, λ, for a Rossby wave in a zonal current satisfies (Pedlosky 1979)

$$\lambda = 2\pi(U/\beta_0)^{\frac{1}{2}} = 2\pi R/\beta^{\frac{1}{2}}$$

or

$$\lambda/R = 2\pi/\beta^{\frac{1}{2}}. \tag{3.1}$$

For the values of β(0.8, 2.0, 0.5 and 1.0) in the examples shown in figures 5b and 6, the theoretical non-dimensional wavelengths λ/R are 7.02, 4.44, 8.89, and 6.28 respectively, though these values are modified when viscous effects are significant (Vaziri & Boyer 1977; Guala 1971). In spite of the difficulties in estimating wavelengths from the photographs (particularly on the left side), measurements demonstrate that they are of the same order as the theoretical values above.

While, as noted, there are clear differences in the overall flow structure between f-plane and westward and eastward β-plane flows, these flows have certain gross features in common. Of these the most noticeable is the occurrence of asymmetry in the separated region downstream of the cylinder; the character of this asymmetry is also similar. These observations concerning flow asymmetry contrast with the non-rotating case (Gerrard 1978; Coutanceau & Bouard 1977) where, in general, for the Reynolds numbers and aspect ratios of the present study the downstream flows exhibit a symmetrical behaviour. An additional point of note is that the filament lines in the steady rotating-flow wake (eastward, westward or f-plane) are not confined to 'their own side' of the cylinder as they are in non-rotating flows.

We have concluded that, qualitatively, the evolution of the downstream eddy structure as given by Boyer (1970) and sketched in figure 2 is valid not only for the f-plane but also for the β-plane westward and eastward flows. That is, for sufficiently small free-stream velocities (i.e. sufficiently small Rossby number) the flow is approximately fully attached. For these cases there is little evidence of eddying motion *per se*. Examples of this flow type for all cases are shown in
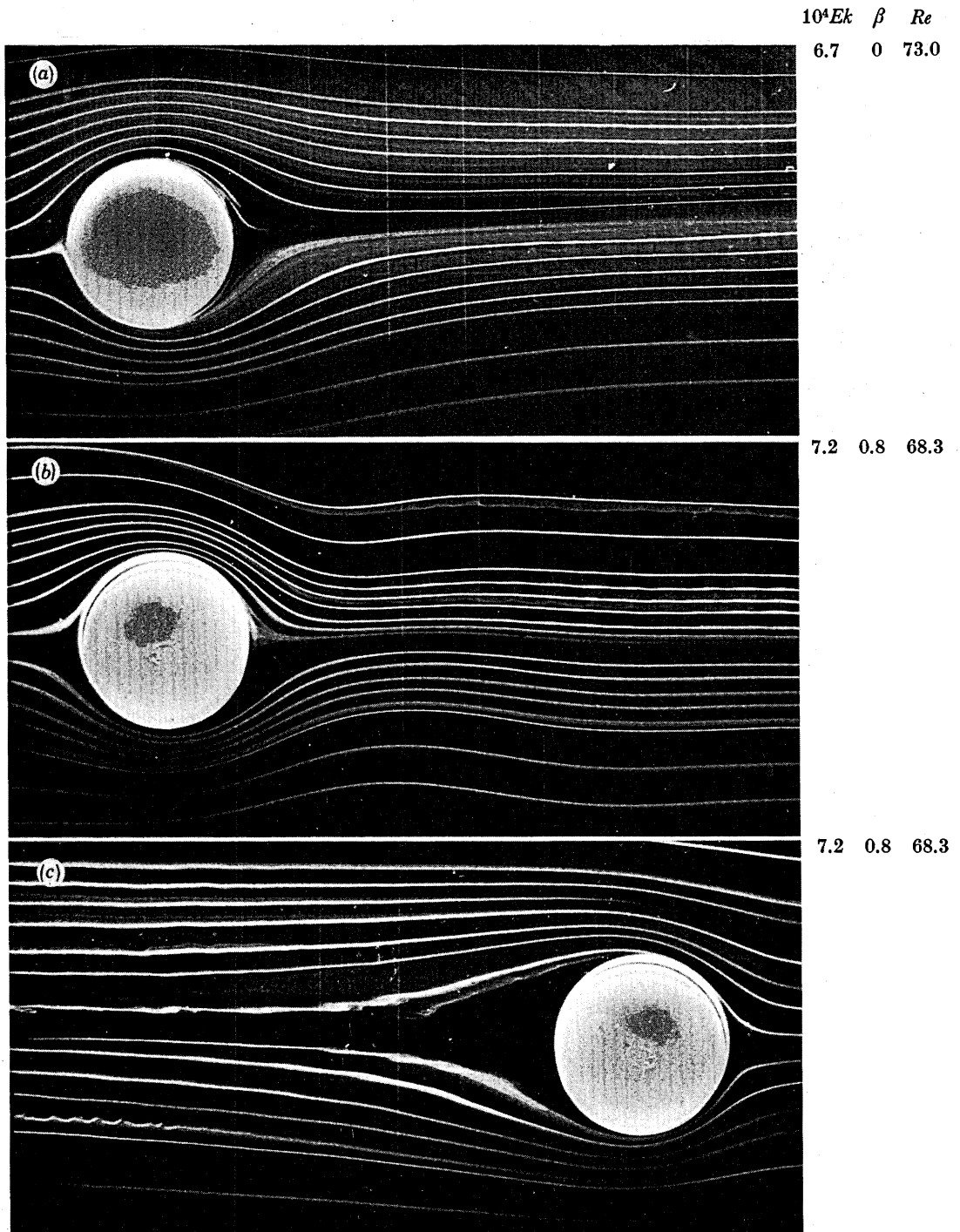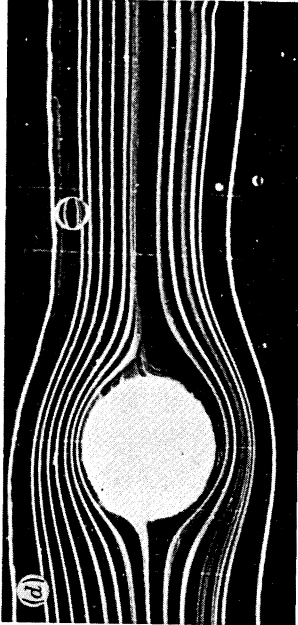
FIGURE 5. Comparison of (*a*) *f*-plane, (*b*) β-plane eastward and (*c*) β-plane westward
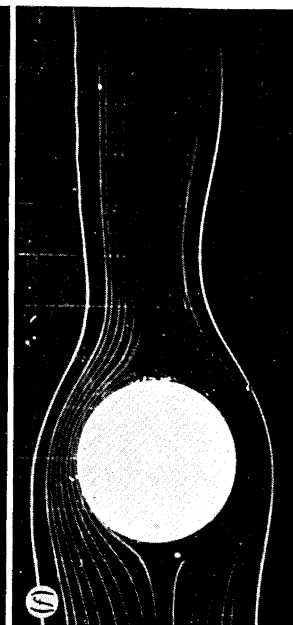plane flow patterns for $Ro = 4.9 \times 10^{-2}$, $R/H = 0.73$.

FIGURE 6. Plan photographs of β-plane eastward flow past a cylinder illustrating flow structure for various Ro, Ek and β. Arrow on (a) indicates the location of the turning point referred to in the text.
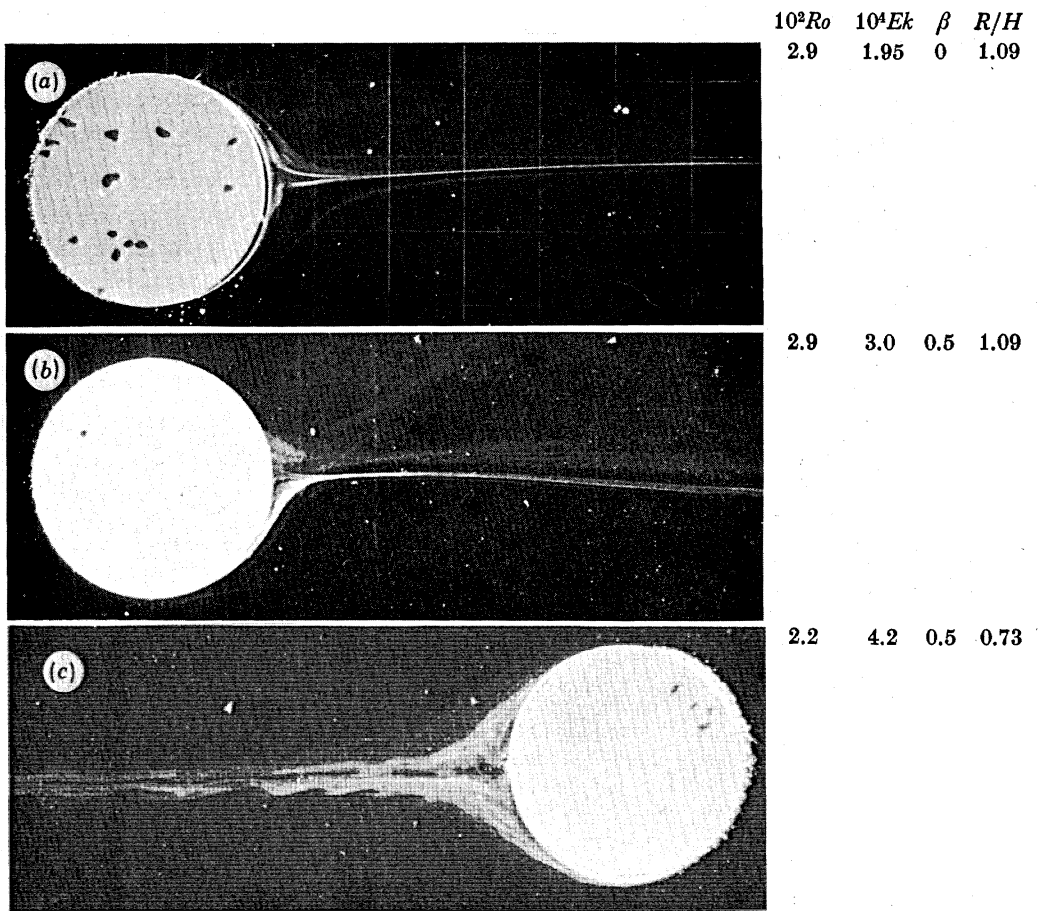
$10^2 Ro$	$10^4 Ek$	β	R/H
2.9	1.95	0	1.09
2.9	3.0	0.5	1.09
2.2	4.2	0.5	0.73

FIGURE 7. Plan photographs illustrating essentially fully attached flow for (a) f-plane,
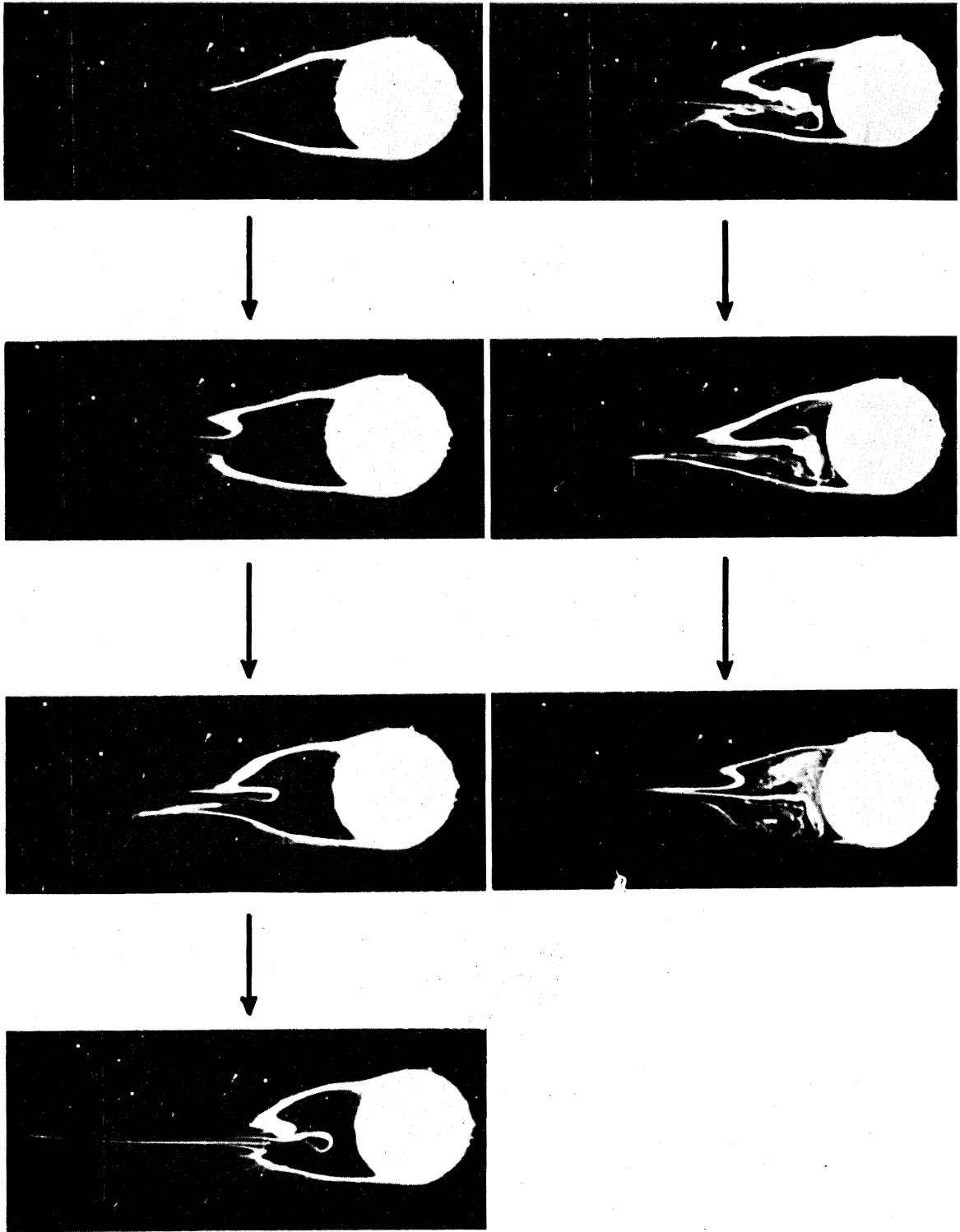(b) β-plane eastward and (c) β-plane westward flows.

FIGURE 8. Time sequence showing double-eddy formation for β-plane westward flow,
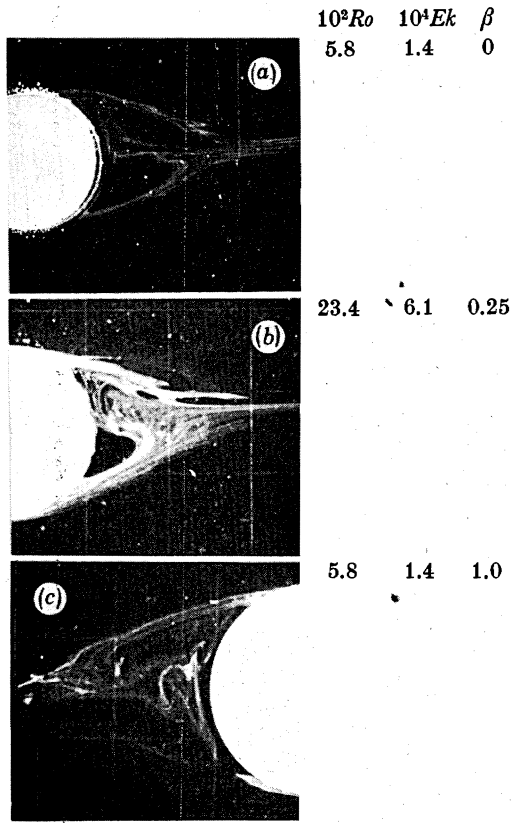for $Ro = 28.9 \times 10^{-2}$, $Ek = 26.4 \times 10^{-4}$, $\beta = 0.05$ and $R/H = 0.36$.

FIGURE 9. Plan photographs illustrating steady double -eddy systems for $R/H = 1.09$: (*a*) *f*-plane, (*b*) β-plane eastward and (*c*) β-plane westward flows.
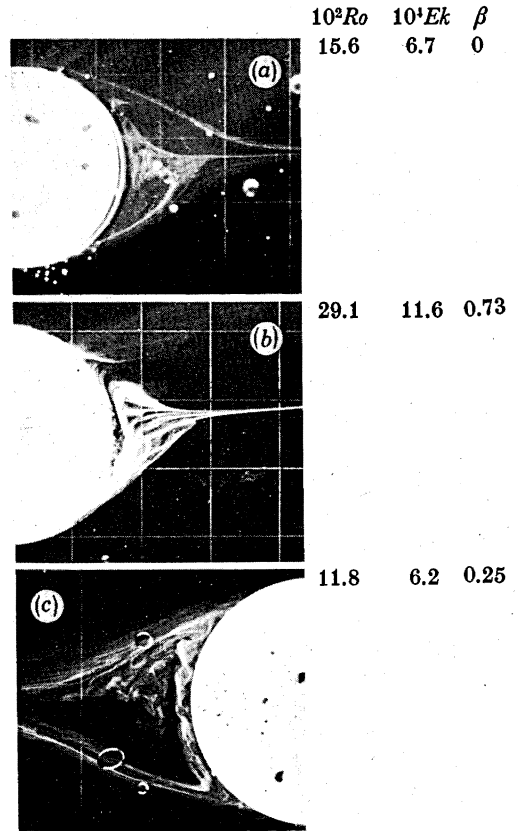
FIGURE 10. Plan photographs illustrating unsteady double-eddy systems for $R/H = 0.73$: (*a*) *f*-plane, (*b*) β-plane eastward and (*c*) β-plane westward flows.
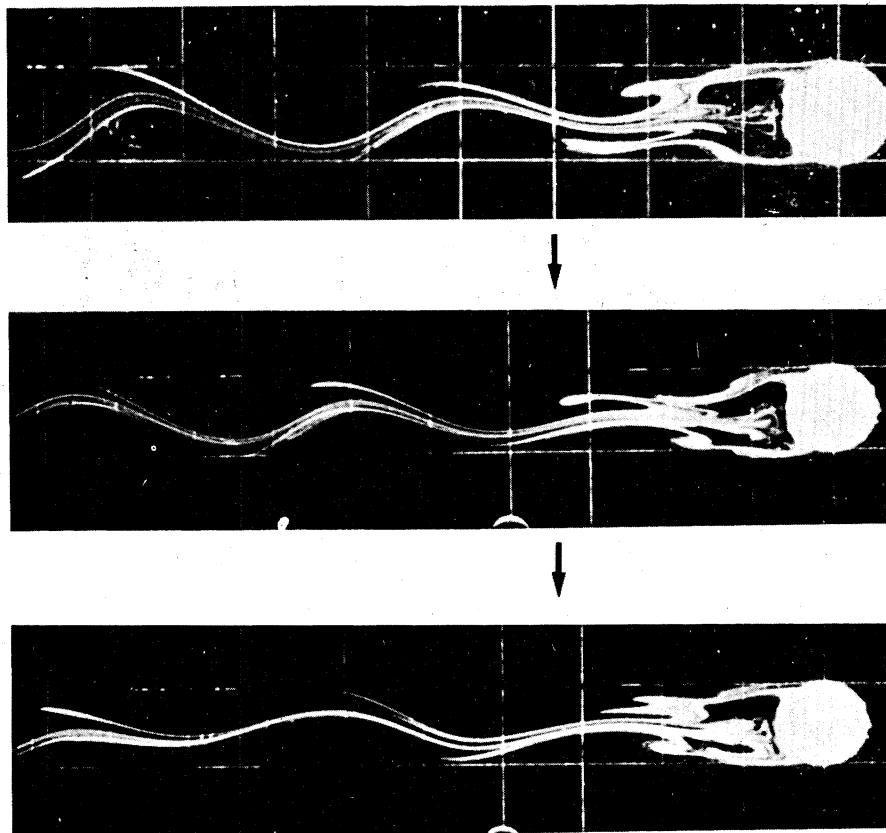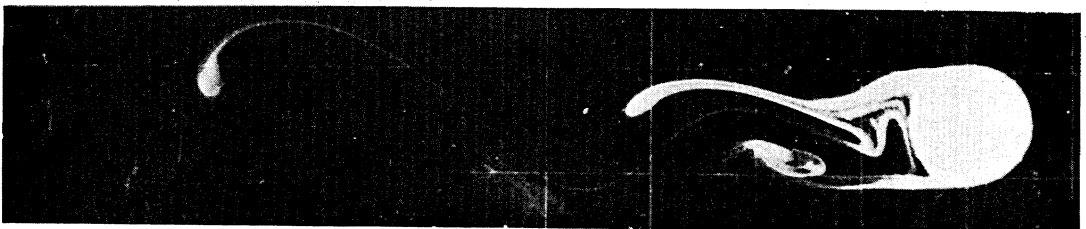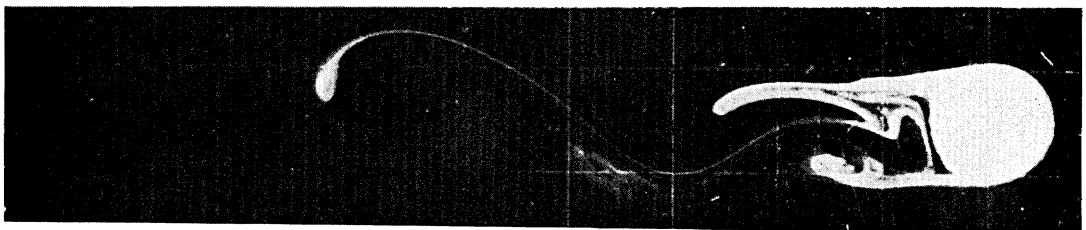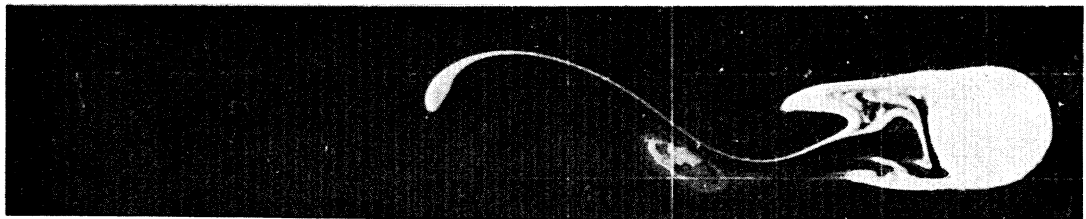

FIGURE 11. Time sequence showing the downstream development of unsteady β-plane westward flow for $Ro = 38.6 \times 10^{-2}$, $Ek = 26.7 \times 10^{-4}$, $\beta = 0.05$ and $R/H = 0.36$.
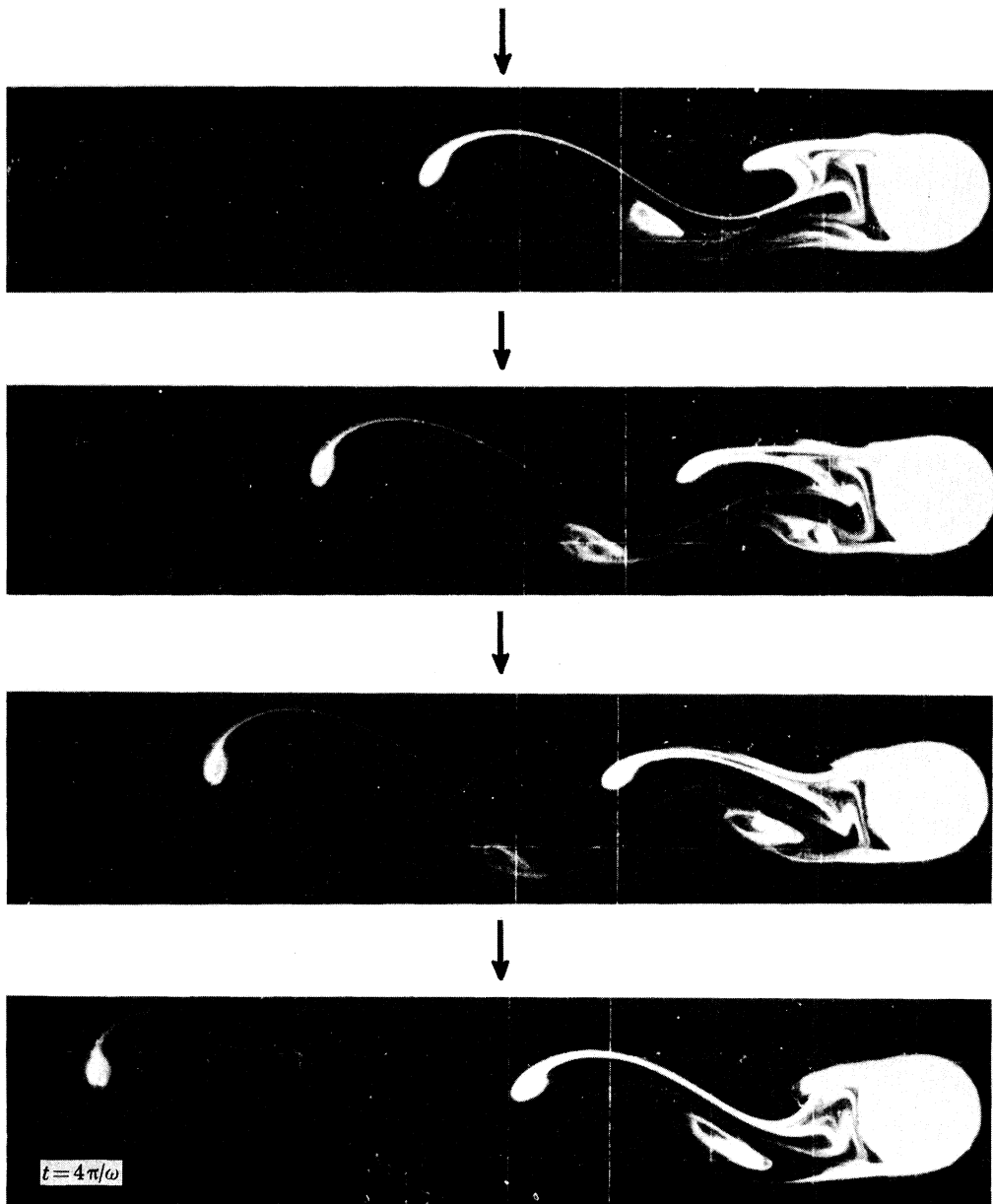
FIGURE 12. Time sequence showing vortex shedding for unsteady β-plane westward flow for $Ro = 81.6 \times 10^{-2}$, $Ek = 51.5 \times 10^{-4}$, $\beta = 0.02$, $R/H = 0.36$. The interval between successive photographs is one quarter of the background rotation period.
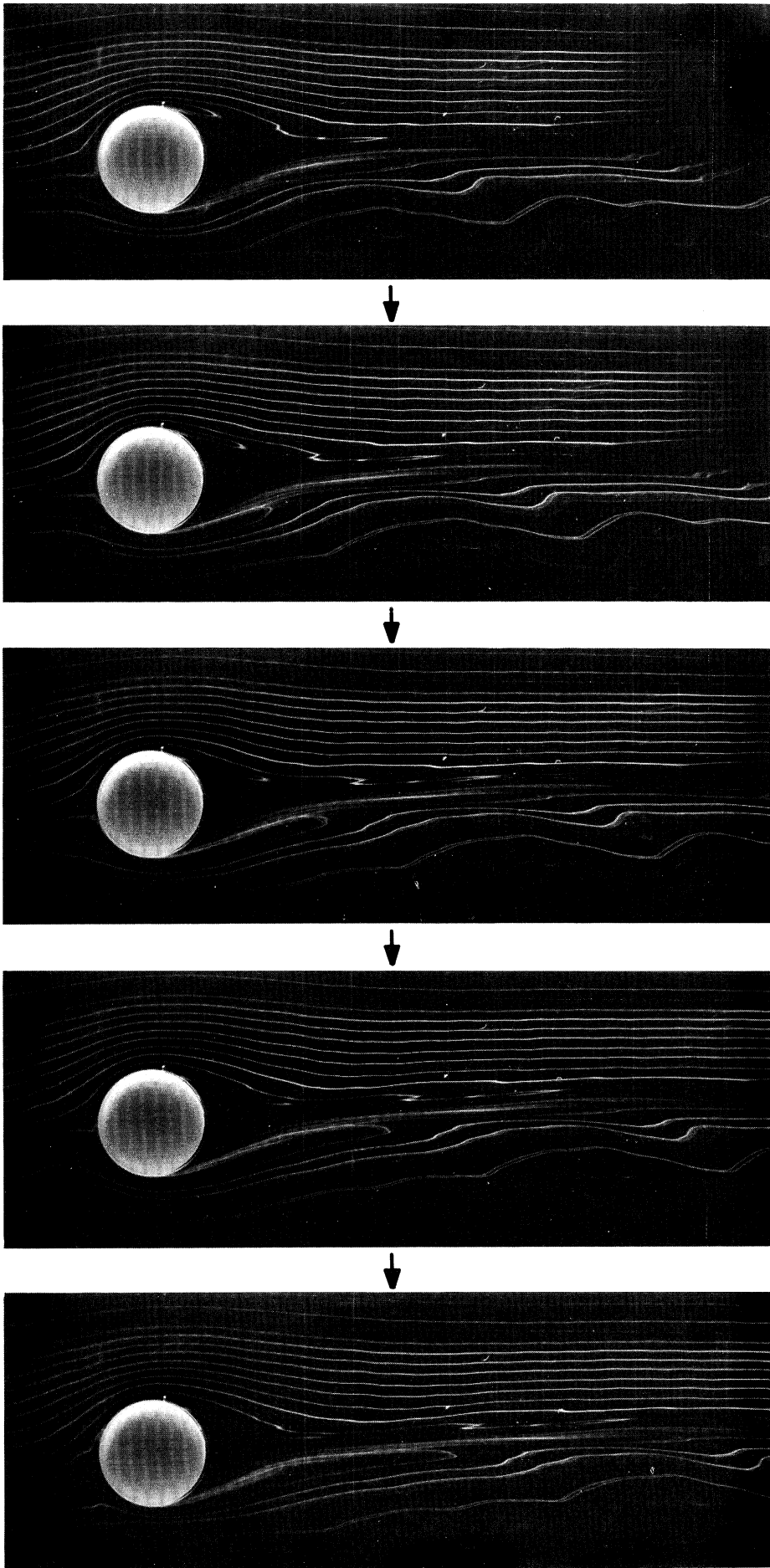
FIGURE 13. For description see opposite.

figure 7 (plate 3). Dye released uniformly around the periphery of the cylinder surface separates asymmetrically, some of the dye at the right rear of the cylinder remaining fully attached until reaching the position corresponding to the rear stagnation point of ideal flow for the non-rotating counterpart. For reasons already discussed, the approximately fully attached flow type is more common with β-plane eastward flows than with others.

As the free-stream speed is increased a steady asymmetric eddy pattern develops in which a large eddy is attached to the right-hand side of the cylinder (facing downstream) with a smaller eddy lying away from and to the left of the cylinder. Figure 8 (plate 4) is a time sequence of photographs showing the development of this double-eddy structure for westward flow. Fluid within the bubble enclosing the eddies is seen to circulate in a cyclonic sense at the right rear of the obstacle and in an anticyclonic sense at the left rear. In figure 9 (plate 5) we show photographs of this double-eddy structure for f-plane and β-plane eastward and westward flows. The qualitative similarity among the experimental runs is clear. Details of the structure depend on specific values of the system parameters as will be discussed further.

At sufficiently high Rossby numbers unsteadiness develops in the double-eddy structure. Figure 10 (plate 5) exemplifies this unsteadiness, for f-plane and eastward and westward flows when both Ro and Ek are large. Note, in particular, the irregular boundary between individual eddies within the separation bubble, a common feature of all unsteady eddy-pair flows (see Boyer (1970) for a description of the f-plane case). An unsteady eddy-pair with a resulting sinuous tail behind the obstacle is revealed by figure 11. In this example, for westward flow, both Ro and Ek are relatively large and the β-effect is relatively weak ($\beta = 0.05$). Note again the asymmetry in both the unsteady eddy-pair and the associated downstream tail.

When both Ro and Ek take higher values than in figure 11 (plate 5) eddy shedding occurs. This is illustrated in figure 12 (plates 6 and 7) where a sequence of photographs taken every quarter of a revolution is displayed. Eddies shed by the obstacle can be followed through the sequence to reveal a periodicity, T, which in this case matches approximately the periodicity of the rotating frame. That is, similar flow features occur at the same distance downstream after each rotation period, T. For this example the Strouhal number, $St = 2R/UT$, takes a value of 0.196.

It is of some interest to compare these results with measured periodicities and Strouhal numbers from satellite data on atmospheric vortex shedding by islands. Such measurements have been made by several authors, including Tsuchiya (1969) and Chopra & Hubert (1964), who both measured eddy periodicities that differed considerably from the local inertial periods, indicating that for this aspect of the flow rotational constraints were not dominant. This is confirmed by the high Rossby numbers appropriate to these investigations (12.7 and 3.6 respectively for the Tsuchiya and Chopra & Hubert studies). Note, however, that in spite of the difficulties in comparing cylindrical obstacles with conical or irregular island topographies, the Strouhal number in the laboratory investigation was close to Strouhal numbers measured from the satellite studies (0.194 and 0.235 respectively). A comparison of figures 11 and 12 confirms the earlier finding that, in contrast to non-rotating flows, the details of rotating flows depend not simply upon

<hr/>

DESCRIPTION OF PLATE 8

FIGURE 13. Time sequence showing the development of unsteady f-plane flow for $Ro = 10.0 \times 10^{-2}$, $Ek = 6.7 \times 10^{-4}$, and $R/H = 0.73$. Note the successive downstream location of identifiable flow features (e.g. the left rear separated eddy).

Reynolds number, Re, but also upon the individual values of Ro and Ek. The values of Re in figures 11 and 12 are almost the same (144 and 158 respectively) but the flow patterns are quite different because of differences in Ro and Ek. Though β also takes a different value in figure 12, it remains close to zero and any effects of its variation from 0.05 to 0.02 will be insignificant here.

More detailed information on the asymmetry in the wake when the separation eddies are unsteady is obtained from photographs taken with dye being released continuously upstream of the cylinder. Figure 13 (plate 8) illustrates this feature for f-plane flow although similar observations were also made for β-plane westward and eastward flows. Some care is required in interpreting such photographs, since they represent streaklines and not streamlines. One notes that in the f-plane sequence there is larger distortion on the right side of the wake. This is consistent with the earlier observation that unsteady separation eddies on the right were larger than those on the left. Examination of successive frames of the f-plane sequence in figure 13 shows how features of the unsteady eddy can be identified as it is advected downstream by the mean flow, without extensive change of shape.

Finally, we note that the asymmetry observed in the laboratory experiments for the unsteady and eddy-shedding régimes is also apparent in some of the satellite images of vortex shedding in the atmosphere (see Lyons & Fujita 1968; Tritton & Davies 1981; and Gjevik 1980). Though the detailed structure of the latter varies considerably from day to day and depends upon both the form of the density profile in the atmosphere and the degree of unsteadiness in the incident flow (Gjevik 1980), it seems that for certain circumstances the similarities between our laboratory results and the atmospheric vortex trails may be more than fortuitous. For example, as pointed out by Scorer (1978), in some circumstances the cyclonic vortices resulting from westerly air flow past the island of Jan Mayen were stronger than their anticyclonic counterparts; see photograph in Scorer (1978). Pitts *et al.* (1977) present a photograph of vortices in the lee of Guadalupe Island off the coast of Baja, California taken from Skylab. This photograph, reproduced here as figure 14 (plate 9), clearly shows strong cyclonic vortices with relatively weak or non-existent anticyclonic motions. These atmospheric observations are noted to be in qualitative agreement with laboratory experiments as exemplified by figure 12.

3.2. *Quantitative measurements*

In assessing individual parameter effects on flow behaviour, efforts were made to identify experimental observables that could be measured from photographic records of the flow. In essence, there are two such observables which serve as suitable and representative indicators:

(i) the angle of separation of the boundary layer on the surface of the cylinder; and

(ii) the length of the separation bubble (i.e. the envelope enclosing the eddies) behind the cylinder (Taneda 1956; Gerrard 1978).

Because of the sensitivity of the separation angles to slight variations in the Rossby number (see for example Merkine & Solan's (1978) theoretical predictions), and the attendant importance of small experimental errors in measuring the free-stream velocity and rotation rate, we were led to adopt the second indicator as the primary observable in the present experiments. Information on the length, form, and structure of the separation bubble was obtained from photographs taken with dye being released continuously from the surface of the cylinder only. Photographs in which streakline patterns were made visible from tracers introduced upstream of the cylinder (e.g. figure 5) were therefore excluded from the separation-bubble measurements.

Figure 15 illustrates schematically the definition adopted for the length of the bubble, for all

steady flows. The dimensional length, ϵ, is defined as the distance from the point, O, at the rear of the cylinder to the point at which the separation, δ, of the two streamlines enclosing the downstream bubble has been reduced to a given arbitrary value. The value chosen was $\frac{1}{5}R$, where R is the radius of the cylinder. All data that include the normalized eddy size, ϵ/R, are based upon the above definition. The separation value, $\delta = \frac{1}{5}R$, is, of course, arbitrary, its choice being dictated by the following two considerations. Firstly, it must define a bubble length that is a representative indicator of the flow structure. Examination of the photographic data confirms that with this choice the essential structure of the bubble is contained within a distance ϵ of point O. Secondly, the values of δ and the associated ϵ must be easily and unambiguously measurable from the projected photographic negatives. (This is not so, for example, if ϵ is defined as the distance
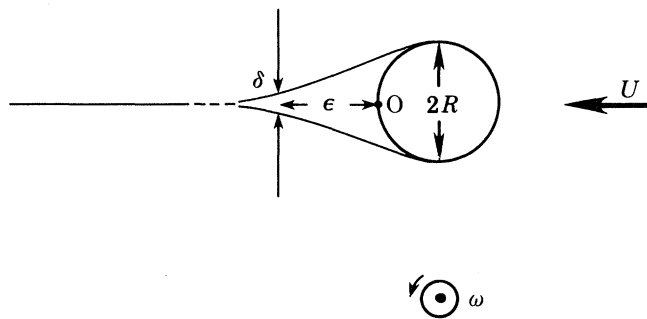

FIGURE 15. Schematic illustration of the definition of separation
bubble length, ϵ. See text for further details.

downstream of the obstacle to the point at which $\delta = 0$.) Chiefly for these reasons, the present definition was adopted. As indicated earlier, measurements of ϵ/R were made directly from photographic negatives of the flow projected onto a screen. In the few cases where the junction of the downstream separation streamlines was displaced from the east–west line passing through the centre of the obstacle, ϵ was still measured from O to the intersection of the east–west centre-line and a north–south line passing through the junction.

With this definition of bubble length, there are two points of detail that must be borne in mind. First, as the previous comment suggests, measurements of ϵ/R reveal nothing about the asymmetry of the eddies. They give an incomplete description of the flow. Indeed, often an important feature of the flow is the difference in separation angles at the right and left of the obstacle respectively, and the difference in shape and extent of separate eddies when formed in pairs at the right and left downstream regions. Secondly, the definition relies upon the efficiency of the flow visualization technique in revealing separation streamlines. Unless precautions are taken to ensure that sufficient tracer is released from the cylinder, the inner streamline separating the two eddies may be identified incorrectly as the left separation streamline for westward flow (and vice versa). In consequence ϵ/R will be underestimated.

Ideally, of course, the definition of fully attached flow, *vis-à-vis* ϵ/R, is that ϵ/R is identically zero. Because of difficulties related to such matters as tracer diffusion near the downstream portion of the cylinder, observational errors caused by insufficient tracer being released into the boundary layers and so on, substantial experimental error enters into the measurement of ϵ/R, especially when the eddy sizes are small. We have thus adopted the rather arbitrary definition that when $\epsilon/R < 0.5$ the flow is 'essentially fully attached'.

3.2.1. Flow on f-plane

Figures 16–18 are plots of separation bubble size as a function of Ro and Ek for cylinder aspect ratios, R/H, of 1.09, 0.78 and 0.36, respectively. The dashed lines on the diagrams represent the approximate locations of ϵ/R-ratios of 1.0, 2.0, and 3.0 (see the figure legends). The solid lines on the diagrams represent the theoretical dividing line between fully attached (below the line) and detached (above the line) flows obtained by Walker & Stewartson (1972) and Merkine & Solan (1979); see relation (1.1). We also note that a tilde above symbols on these and subsequent
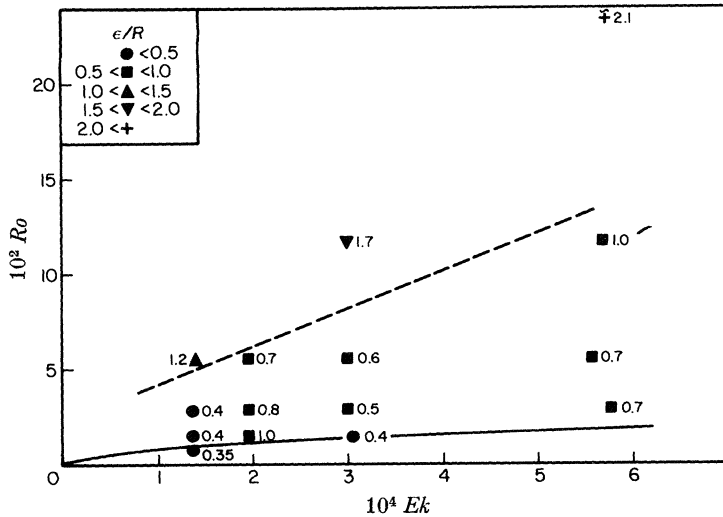

FIGURE 16. Ro:Ek régime diagram showing (numbers) measured values of ϵ/R for f-plane flow with $R/H = 1.09$. The dashed line indicates the estimated division between $\epsilon/R < 1.0$ and $\epsilon/R > 1.0$ and the solid curve is the theoretical prediction (Walker & Stewartson 1972; Merkine & Solan 1979) delineating the limits for fully attached flow (see text). In this and subsequent figures a tilde over a symbol represents experimental runs in which unsteadiness was observed in part of the downstream flow field.
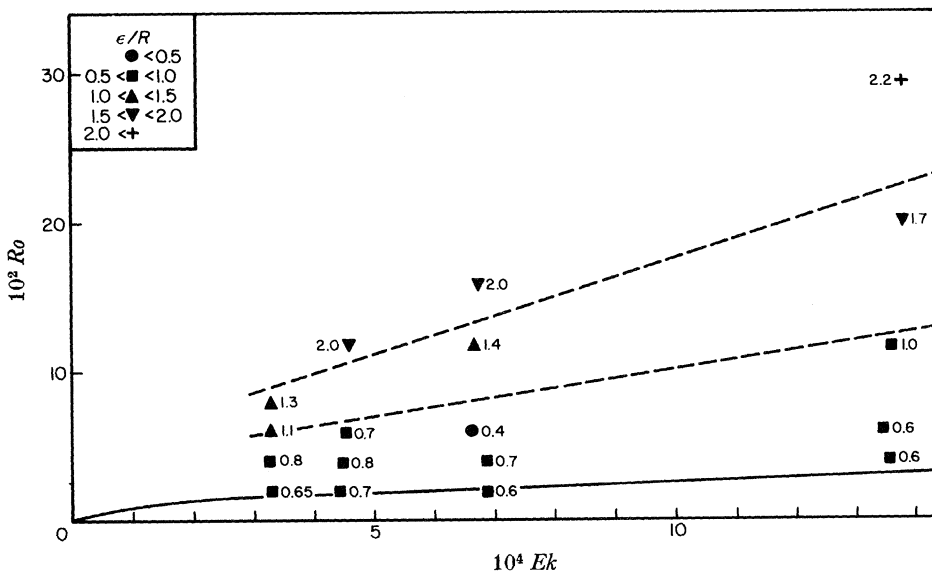

FIGURE 17. Ro:Ek régime diagram showing measured values of ϵ/R for f-plane flow with $R/H = 0.73$. The lower and upper dashed lines indicate the estimated division between $\epsilon/R < 1.0$ and $\epsilon/R > 1.0$ and between $\epsilon/R < 2.0$ and $\epsilon/R > 2.0$ respectively; solid curve as in figure 16.

plots represents experimental runs in which unsteadiness was observed in a portion of the down-stream flow field; see for example figures 11 and 12.

We first note that the régime diagrams represented by figures 16–18 are similar to those given by Boyer (1970). However, the present observational data are more quantitative in the sense that specific bubble sizes are determined. The qualitative findings of the present and earlier studies are the same. While numerous experimental runs were made near the theoretical line for separation, only a few experiments actually were on or below this line. Within the limitations of the experiments and the theory, however, one can conclude that there is good agreement between theory and experiment. As noted earlier, Leibovich (1967) predicts that separation will occur and that the flow is inherently unsteady for the Rossby-number range given by (1.2). Experimentally, we have found the flow to be steady and essentially fully attached in this Rossby-number range.
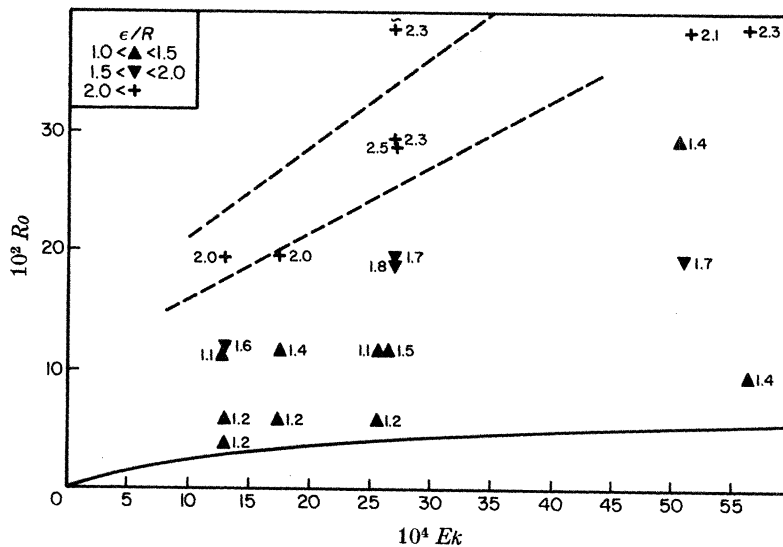

FIGURE 18. $Ro:Ek$ régime diagram showing measured values of ϵ/R for f-plane flow with $R/H = 0.36$. The lower and upper dashed lines indicate estimated divisions between $\epsilon/R < 2.0$ and $\epsilon/R > 2.0$ and between $\epsilon/R < 3.0$ and $\epsilon/R > 3.0$ respectively; solid curve as in figure 16.

Variation of bubble size with Rossby number. Each of figures 16–18 clearly indicates that the bubble size increases monotonically with increasing Rossby number, the remaining system parameters being fixed (for example all dimensional parameters fixed with the exception of increasing free-stream speed). This is in consonance with our intuition and with the existing results (Taneda 1956) on non-rotating flow past a cylinder which show that the bubble size increases with increasing Reynolds number. This increase in bubble size with Rossby number is demonstrated by the series of photographs for f-plane flow in figure 19 (plate 10).

Variation with Ekman number. Figures 16–18 also show that the bubble size increases with decreasing Ekman number, the remaining system parameters being fixed. For the parameter ranges considered it is noted that the change in bubble size is not as sensitive to variations in Ek as it is to changes in Ro.

Variation with R/H. For the lower values of the Rossby and Ekman numbers in figures 16 and 17 we note the tendency for the bubble lengths to increase with decreasing R/H, the remaining system parameters being fixed; note, however, the scale differences on the figures.

3.2.2. *Flow on β-plane*

For β-plane flows the additional parameters, β, and the flow direction also govern the bubble size. The bubble size data are not as simply represented as those for the f-plane.

Figures 20–22 are plots of ϵ/R against Ro for cylinders having aspect ratios, R/H, of 1.09, 0.73 and 0.36 respectively. For each of the plots the Ekman number is approximately the same and ϵ/R-dependence on β and flow direction in addition to that on Ro are depicted; note that temperature variations of the working fluid produce slight viscosity changes which in turn cause variations in Ek; hence the indication of Ekman-number variations in the various experiments on the figures. Figures 20–22 enable one readily to discuss bubble-size dependence on flow direction, Rossby number, β, and R/H. To examine the dependence on Ek it is found convenient to replot the data in the form ϵ/R against Ek; see figures 23–25.
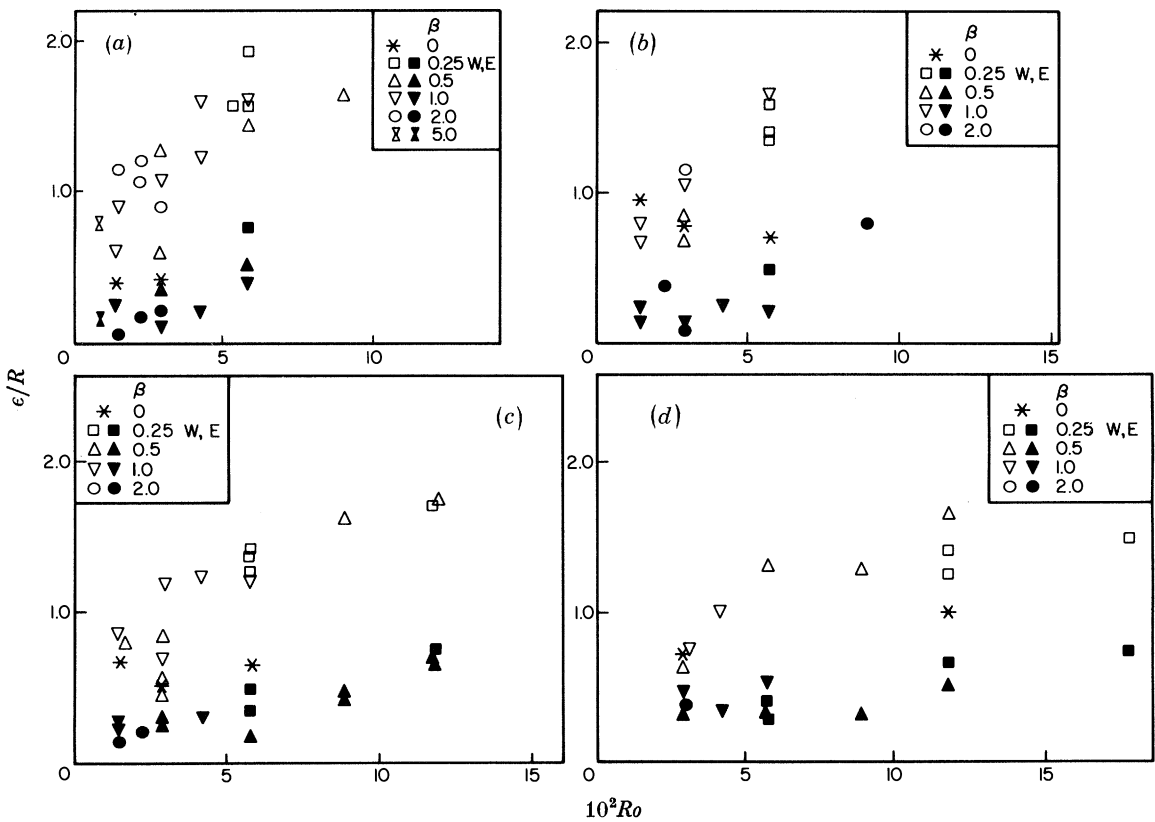

FIGURE 20. Plots of ϵ/R against Ro, β and flow direction for $R/H = 1.09$ and Ek-values (*a*) $(1.5 \pm 0.1) \times 10^{-4}$, (*b*) $(2.0 \pm 0.1) \times 10^{-4}$, (*c*) $(3.0 \pm 0.2) \times 10^{-4}$ and (*d*) $(6.0 \pm 0.5) \times 10^{-4}$. E and W signify eastward (prograde) and westward (retrograde) flow directions respectively.

Variation of bubble size with flow direction. A common, and clearly the most apparent, feature of all of the plots in figures 20–25, is the clear division of the data into f-plane and β-plane eastward and westward categories (asterisk, solid and open symbols respectively). The data show that under otherwise identical conditions bubble sizes are largest for westward flow, smallest for eastward flow and intermediate for the f-plane. These eddy-size distinctions apparently become less pronounced at high Ekman numbers; see figure 22*d*. We note, however, that in figure 22*d* the β-values are relatively small, a factor that is probably responsible for the lack of east–west
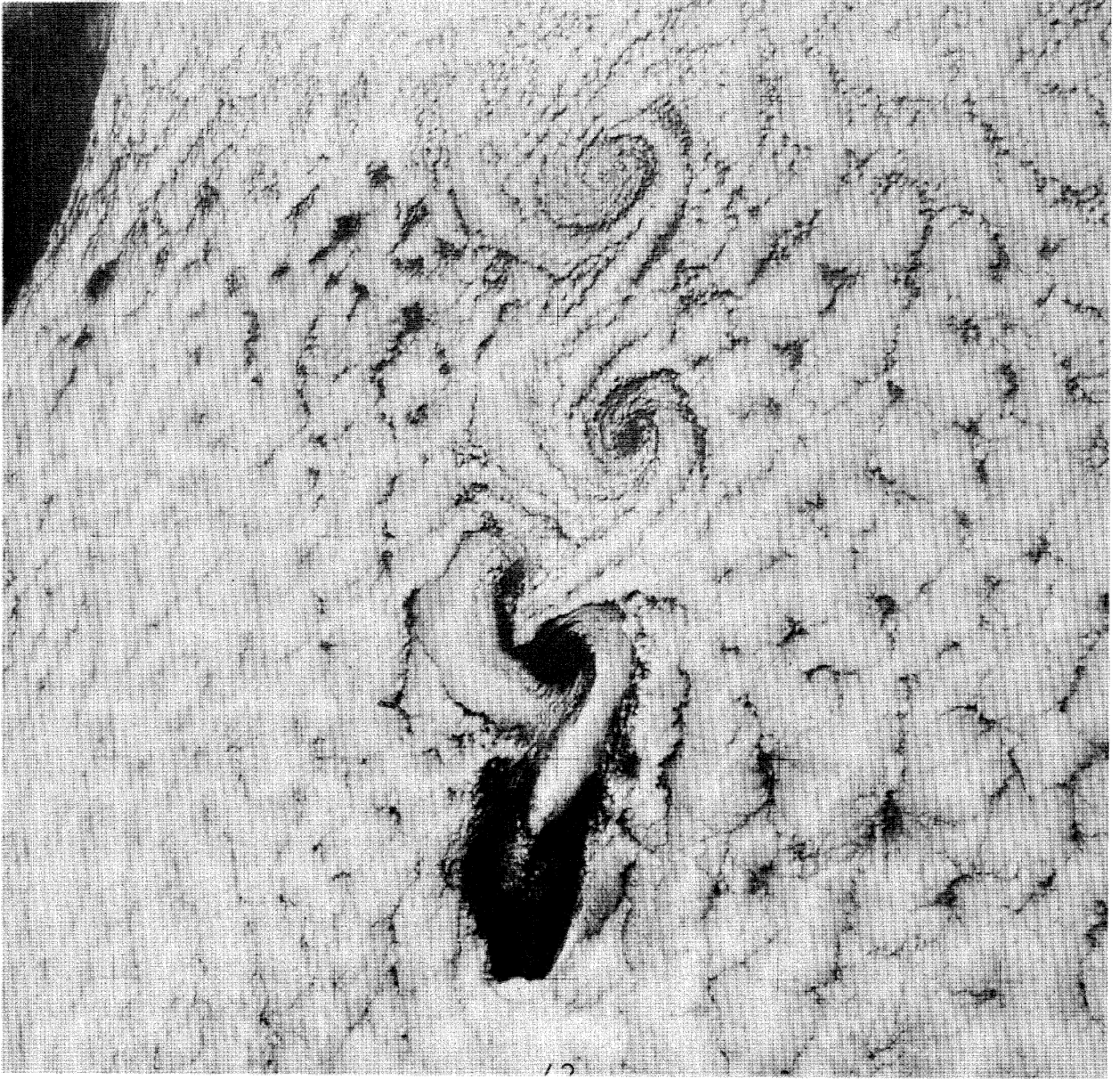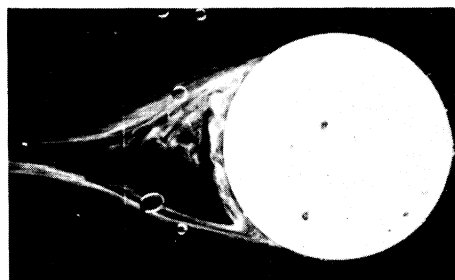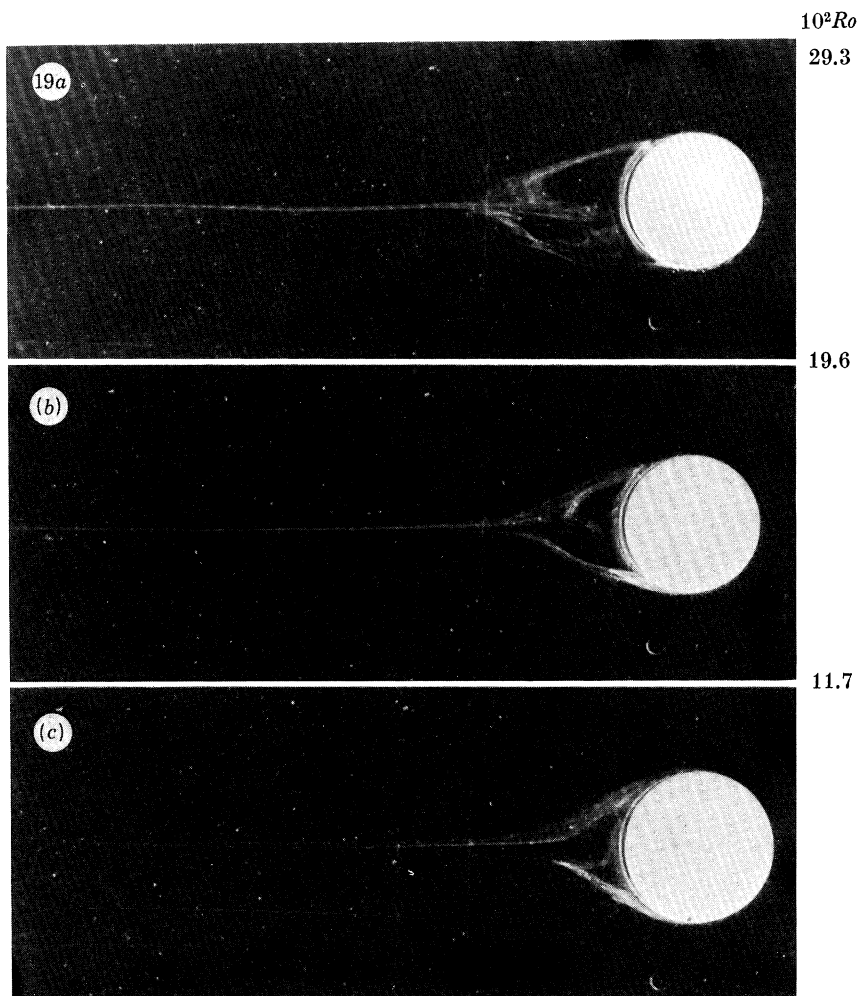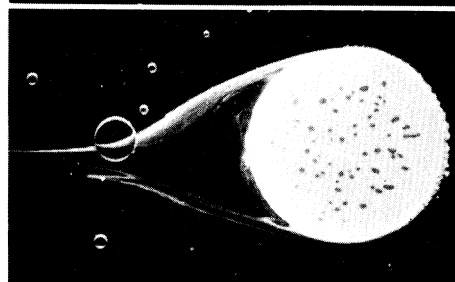
FIGURE 14. Vortex-street cloud pattern in the lee of Guadalupe Island photographed by Skylab (from Pitts *et al.* 1977). Note the dominance of the cyclonic vortices.

Phil. Trans. R. Soc. Lond. A, volume 306

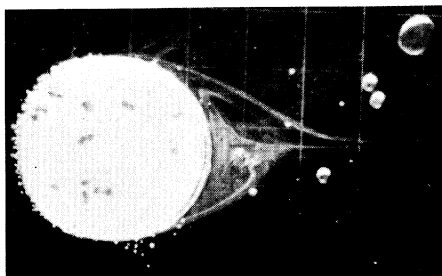*Boyer & Davies, plate* 10

$10^2 Ro$
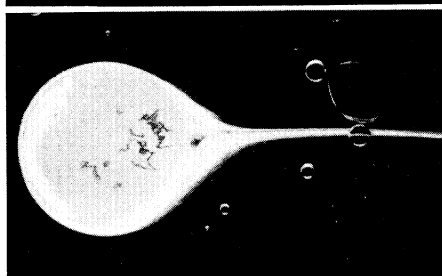

29.3

19.6

11.7

$\beta = 1.0$, westward

$\beta = 0$ eastward

$\beta = 0.25$, westward

$\beta = 0.25$, eastward

$\beta = 0$ westward

$\beta = 1.0$, eastward

FIGURES 19 and 26. For description see opposite.

polarity. Unfortunately, the limitations of the experimental apparatus precluded investigation with high-Ek, high-β combinations. With the exception of figure 22d all of the data show that for identical R/H, Ro and Ek the eddy size increases as the flow type changes from β-plane eastward through f-plane to β-plane westward.

Variation with Rossby number. Figures 20–22 show clearly the increase in eddy size with increasing Rossby number for all flows and all obstacles. The increase in eddy size with Ro is more marked
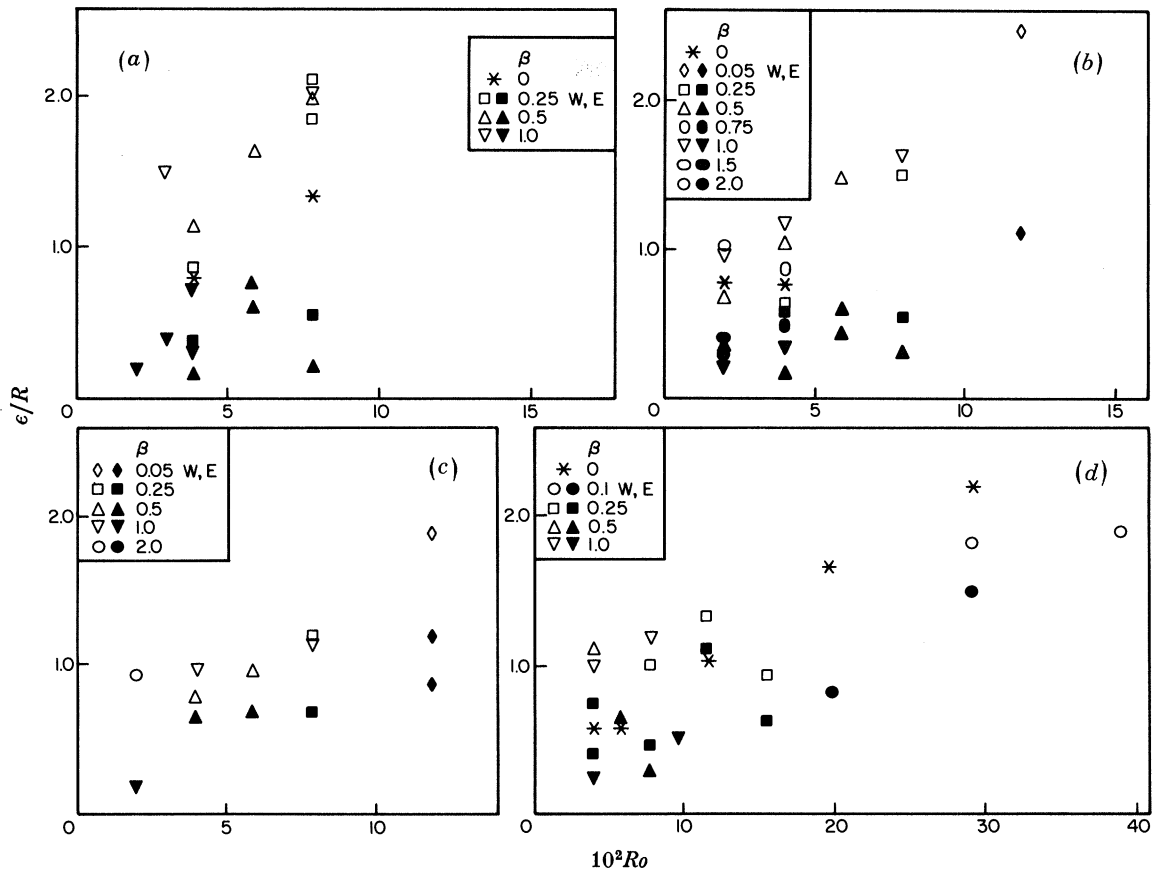

FIGURE 21. Plot of ϵ/R against Ro, β and flow direction for $R/H = 0.73$ and Ek-values
(a) $(3.0 \pm 0.4) \times 10^{-4}$, (b) $(4.5 \pm 0.5) \times 10^{-4}$, (c) $(6.0 \pm 0.5) \times 10^{-4}$ and (d) $(13.0 \pm 1.5) \times 10^{-4}$.

for westward flow than for f-plane or eastward flow, but the overall tendency is present for all of these flows. Again, for practical reasons there were limitations on the possible ranges of Ro and Ek available for specific β and R/H. As a result, a particular symbol for eastward or westward flow can be followed on figures 20–22 only over a restricted range of Ro on a given plot and over only a limited number of R/H-values. Nevertheless, the increase in ϵ/R with Ro is clear for all flow groupings. Recall that this Ro tendency was shown previously for the f-plane in figure 19.

DESCRIPTION OF PLATE 10

FIGURE 19. Plan photographs illustrating the increase in separation bubble size with increasing Ro for f-plane flow with $Ek = 13.8 \times 10^{-4}$ and $R/H = 0.73$.

FIGURE 26. Photographs showing effects of β and flow direction upon the size of the separation bubble for $Ro = 5.8 \times 10^{-2}$, $Ek = 1.5 \times 10^{-4}$ and $R/H = 1.09$.

Variation with β. The influence upon eddy size of changing β can also be ascertained from figures 20–22. For a given Rossby number, Ekman number and aspect ratio, the tendency is for the eddy size (a) to increase with increasing β for westward flow; and (b) to decrease with increasing β for eastward flow. The photographs given in figure 26 (plate 10) of downstream eddies for sequentially varying β for westward and eastward flows clearly demonstrate this β-dependence. Note that starting from a relatively high value of β for eastward flow the eddy region grows
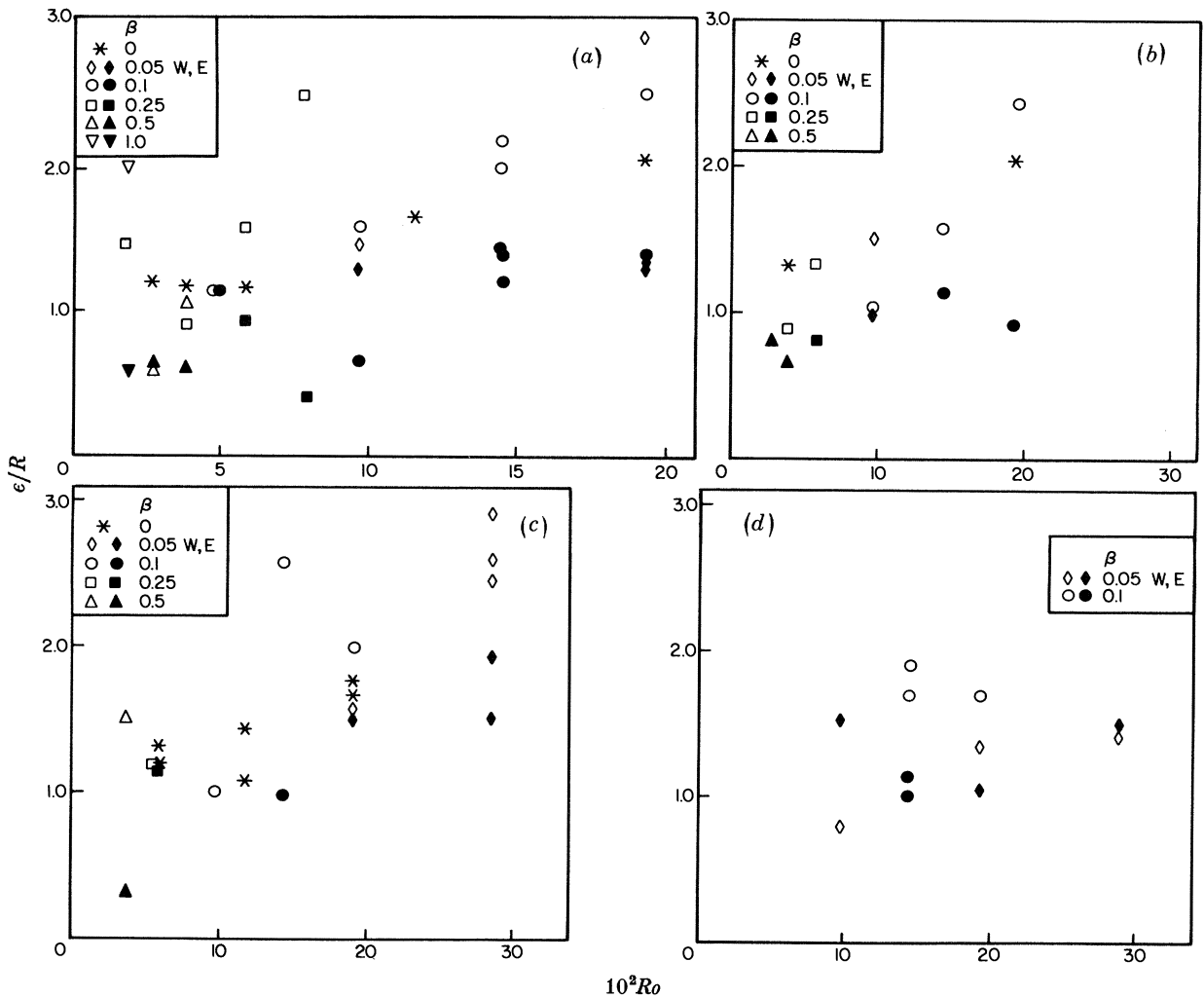

FIGURE 22. Plots of ϵ/R against Ro, β and flow direction for $R/H = 0.36$ and Ek-values
(a) $(13.0 \pm 1.5) \times 10^{-4}$, (b) $(17.5 \pm 2.0) \times 10^{-4}$, (c) $(25.0 \pm 2.0) \times 10^{-4}$ and (d) $(55.0 \pm 5.0) \times 10^{-4}$.

continuously as β is reduced to zero and then, as the direction of flow changes to westward, increases again (figures 26 f–a). This behaviour is shown in many instances on the quantitative plots of figures 20–22; see for example figure 20 b for $Ro \approx 6.0 \times 10^{-2}$ and figure 20 d for $Ro \approx 12.0 \times 10^{-2}$.

Variation with R/H. A comparison of figures 20 and 21 and figures 21 and 22 illustrates the influence of cylinder aspect ratio on eddy size. The plots indicate that for both f-plane and β-plane westward flows the eddy size increases with decreasing R/H, for otherwise identical parameters. A similar indication for β-plane eastward flow is apparent in figures 21 d and 22 a but
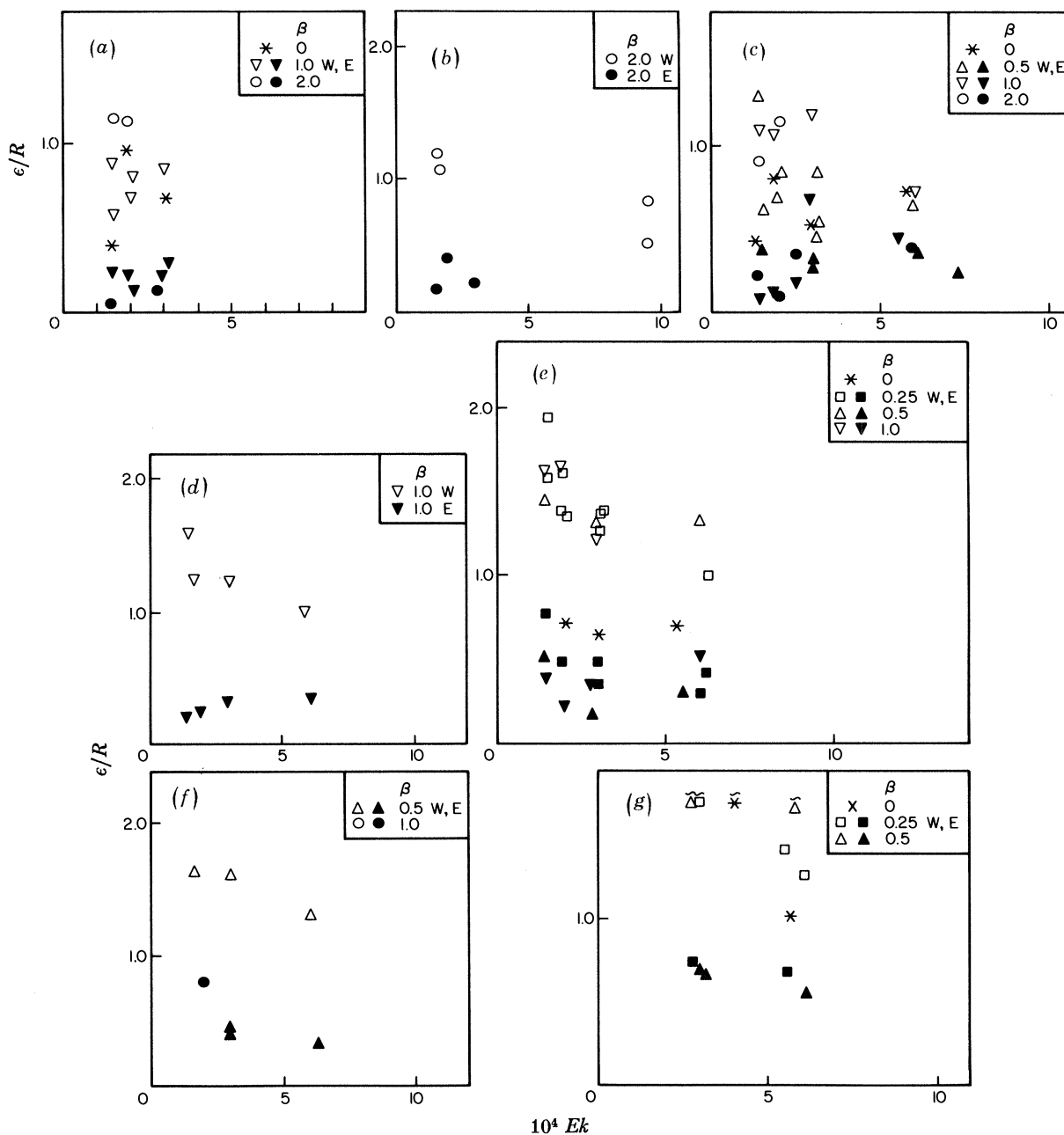
FIGURE 23. Plots of ϵ/R against Ek, β and flow direction for $R/H = 1.09$ and Ro-values (a) 1.4×10^{-2}, (b) 2.2×10^{-2}, (c) 2.9×10^{-2}, (d) 4.2×10^{-2}, (e) 5.8×10^{-2}, (f) 8.9×10^{-2} and (g) 11.8×10^{-2}.

the evidence of this behaviour is not as strong in this case as for the others. Effects of varying R/H are difficult to discern because the degree of overlap of Ro, Ek and β for different cylinders is so limited (see figure 4). Nevertheless, the trends outlined above are supported by the data for a relatively large range of Ro, Ek and β combinations.

Variation with Ek. Bubble-size dependence on the Ekman number can be ascertained from figures 23–25. A characteristic feature of the plots is the decrease in ϵ/R with increasing Ek, for f-plane and β-plane westward flows. This tendency is observed for all aspect ratios and all values of β, except for the lowest values of Ro in each R/H sequence (figures 23a, 24a and 25a).
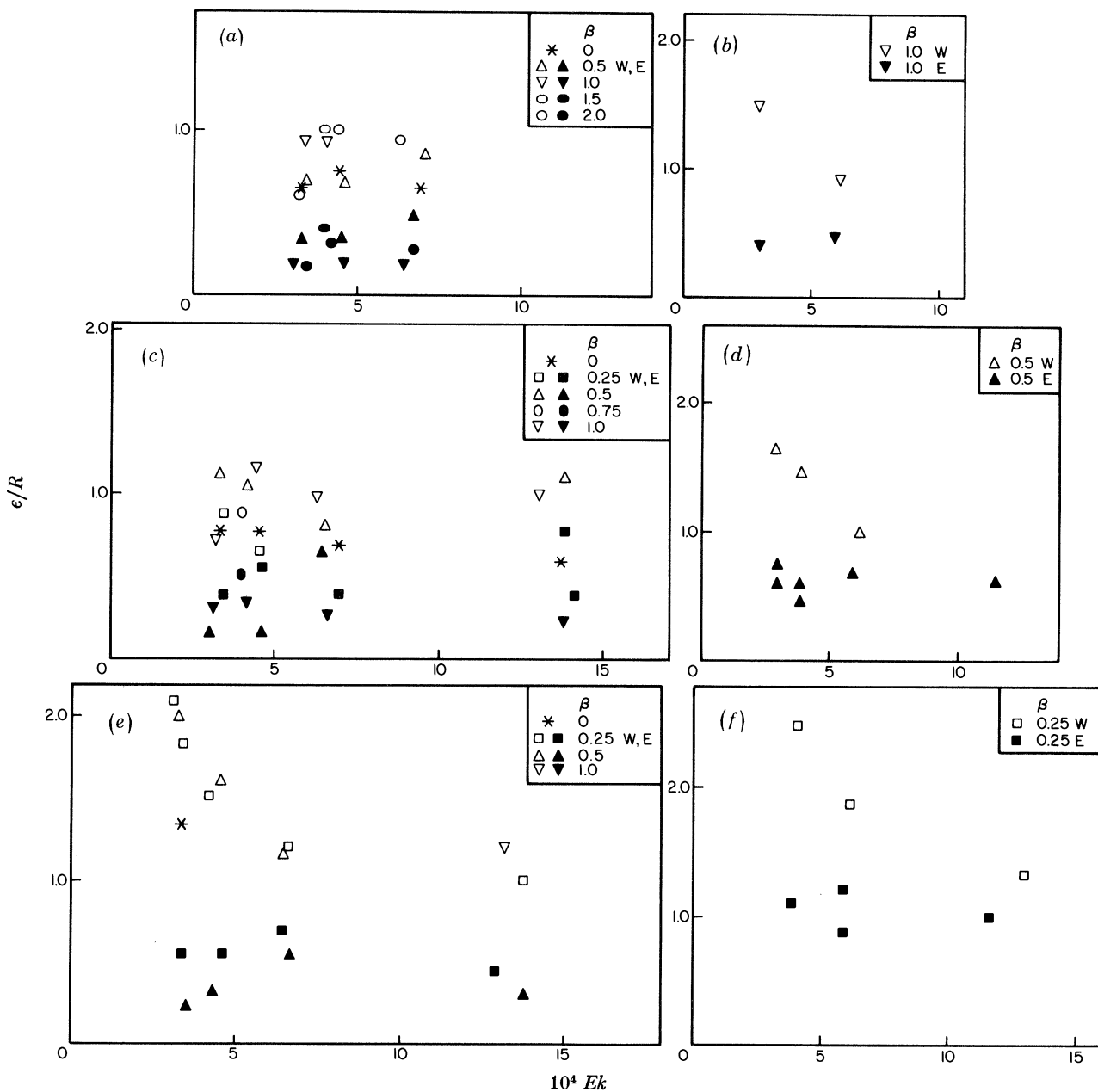
FIGURE 24. Plots of ϵ/R against Ek, β and flow direction for $R/H = 0.73$ and Ro-values (a) 1.97×10^{-2}, (b) 2.95×10^{-2}, (c) 3.93×10^{-2}, (d) 5.9×10^{-2}, (e) 7.9×10^{-2} and (f) 11.8×10^{-2}.

The behaviour for a particular value of β can be followed on all plots; figures $23\,b$, d; $24\,b$, d, f; and $25\,b$, d, and f, however, illustrate the tendency most clearly. Though for westward flow each of these figures shows eddy-size reductions with Ekman number for a single value of β, the values of β vary between plots. The overall trend for westward flow is also confirmed on the remaining composite plots. For the range of parameters investigated, the β-plane eastward bubble sizes are relatively insensitive to changes in Ekman number, except at higher Rossby numbers, where the bubble size may become slightly smaller as the Ekman number increases.

Though the most dramatic variation of ϵ/R with Ek is seen with β-plane westward flows, the

FIGURE 25. Plots of ϵ/R against Ek, β and flow direction for $R/H = 0.36$ and Ro-values (a) 3.86×10^{-2}, (b) 5.8×10^{-2}, (c) 9.65×10^{-2}, (d) 14.5×10^{-2}, (e) 19.3×10^{-2} and (f) 28.9×10^{-2}.

f-plane data points on figures 23–25 also show a reduction in eddy size with increasing Ekman number, for all R/H, particularly at the higher Rossby numbers; see also figures 16–18.

We note finally that instances of unsteady flow are indicated on a number of the figures. They serve to illustrate again the importance of both Rossby number and Ekman number in determining unsteadiness in the wake of the obstacle. This contrasts with non-rotating flow where the flow behaviour is determined primarily by the Reynolds number, the ratio of these parameters. For example, in figure 23g unsteady westward flows are observed for $\beta = 0.5$ and 0.25 for $Ek = 5.82 \times 10^{-4}$ and 2.93×10^{-4} respectively. For the Rossby number considered, the above data points correspond to Reynolds numbers of 203 and 403 respectively. However, in figure 23f for $\beta = 0.5$ and a lower Rossby number the westward flow is steady, even though the Reynolds numbers for some of these points exceed the previous values.

4. SUMMARY AND CONCLUSIONS

The extensive experimental investigation described in the preceeding sections has revealed several unexpected results. Of these the most dramatic has been the difference between westward and eastward flows. The latter is characterized by downstream pinching and bunching whereas the former more closely resembles the f-plane flow past a solid cylinder in which the streamline patterns for essentially fully attached flow approximate those for potential flow past a cylinder.

For the f-plane studies the experiments tend to support the criterion for fully attached flow advanced by Walker & Stewartson (1972) and later by Merkine & Solan (1979); i.e. $R_0 \leqslant (R/H)(\frac{1}{2}Ek)^{\frac{1}{2}}$. The experiments do not support the prediction (Leibovich 1967) that the flow will separate but not contain a reverse flow for the parameter range given by

$$\frac{1}{2}\frac{R}{H}\left(\frac{Ek}{2}\right)^{\frac{1}{2}} \leqslant Ro \leqslant \frac{R}{H}\left(\frac{Ek}{2}\right)^{\frac{1}{2}}.$$

The experiments indicate that for eastward flow the β-effect tends to inhibit flow separation. This observation is in consonance with the predictions of Merkine (1980). Caution must be exhibited, however, because the region of parameter space considered in the experiments is not the same as that required by the theory.

In all steady flows there is asymmetry in the eddy structure downstream of the cylinder though the downstream extent of the bubble enclosing the eddies is much greater for β-plane westward flow than for f-plane and β-plane eastward flows. When the flow becomes unsteady the asymmetry persists.

The occurrence of unsteady flows (whether restricted to the attached eddy region or in the wake as a whole) has been shown to depend primarily upon the individual values of Ro and Ek and not, as in non-rotating flow, solely upon Reynolds number. When eddy shedding does occur cyclonic eddies are substantially stronger than anticyclonic ones.

When the flow around the cylinder separates, the size of the separation bubble region

(i) increases with increasing Ro, for all β, Ek, R/H and for both eastward and westward flows;

(ii) increases with increasing β for westward flow and decreases with increasing β for eastward flow;

(iii) decreases with increasing R/H for westward and f-plane flow;

(iv) decreases with increasing Ek for westward and f-plane flows.

REFERENCES

Baines, P. G. & Davies, P. A. 1980 Laboratory studies of topographic effects in rotating and/or stratified fluids. In *Orographic effects in planetary flows* (ed. R. Hide & P. W. White), pp. 233-299, GARP Publications Series no. 23. Geneva: World Meteorological Organization.

Batchelor, G. K. 1970 *An introduction to fluid dynamics.* Cambridge University Press.

Berger, E. & Wille, R. 1972 Periodic flow phenomena. *A. Rev. Fluid Mech.* **4**, 313-340.

Boyer, D. L. 1970 Flow past a right circular cylinder in a rotating frame. *J. bas. Engng* **92**, 430-436.

Buckmaster, J. 1969 Separation and magnetohydrodynamics. *J. Fluid Mech.* **38**, 481-498.

Buckmaster, J. 1971 Boundary layer structure at a magnetohydrodynamic rear stagnation point. *Q. Jl. mech. appl. Math.* **24**, 373-386.

Chopra, K. P. & Hubert, L. F. 1964 Kármán vortex streets in the Earth's atmosphere. *Nature, Lond.* **203**, 4952, 1341-1343.

Coutanceau, M. & Bouard, R. 1977 Experimental determination of the main features of the viscous flow in the wake of a circular cylinder in uniform translation. Part 1. Steady flow. *J. Fluid Mech.* **79**, 231-356.

GARP 1978 *Report of the First Planning Meeting on the GARP Mountain Sub-Programme.* Geneva: World Meteorological Organization.

Gerrard, J. H. 1978 The wake of cylindrical bluff bodies at low Reynolds number. *Phil. Trans. R. Soc. Lond.* **288**, 351-382.

Gjevik, B. 1980 Orographic effects revealed by satellite pictures: mesoscale flow phenomena. In *Orographic effects in planetary flows* (ed. R. Hide & P. W. White), pp. 302-317, GARP Publications Series no. 23. Geneva: World Meteorological Organization.

Greenspan, H. P. 1968 *The theory of rotating fluids.* Cambridge University Press.

Guala, J. R. 1971 Bottom topography effects on ocean currents. Ph.D. Dissertation, University of Delaware.

Hogg, N. G. 1980 Effects of bottom topography on ocean currents. In *Orographic effects in planetary flows* (ed. R. Hide & P. W. White), pp. 167-205, GARP Publications Series No. 23. Geneva: World Meteorological Organization.

Honji, H. & Ishi-i, K. 1976 Wake shedding from a distorted cylinder. *J. Phys. Soc. Japan* **41**, 3, 1089-1090.

Honji, H., Taneda, S. & Tatsuno, A. 1980 Some practical details of the electrolytic precipitation method of flow visualisation. *Res. Inst. Appl. Mech. Kyushu Univ.* **28**, 89, 83-89.

Hsueh, Y. A. & Legeckis, R. 1973 Western intensification in a rotating water tunnel. *Geophys. Fluid Dyn.* **5**, 333-358.

Imberger, J. & Johannes, R. E. 1981 New island wake form described by native fisherman, yields estimate of horizontal exchange. Unpublished manuscript.

Leibovich, S. 1967 Magnetohydrodynamic flow at a rear stagnation point. *J. Fluid Mech.* **29**, 401-413.

Long, R. R. 1952 The flow of a liquid past a barrier in a rotating spherical shell. *J. Met.* **9**, 187-199.

Lyons, W. A. & Fujita, T. 1968 Mesoscale motions in oceanic stratus as revealed by satellite data. *Mon. Weath. Rev.* (Am. Met. Soc.) **96**, 304-314.

McCartney, M. S. 1975 Inertial Taylor columns on a beta plane. *J. Fluid Mech.* **68**, 71-95.

Merkine, L. O. & Solan, A. 1979 The separation of flow past a cylinder in a rotating system. *J. Fluid Mech.* **92**, 381-392.

Merkine, L. O. 1980 Flow separation on a beta plane. *J. Fluid Mech.* **99**, 399-409.

National Research Council, Italy, Laboratory for the Study of the Dynamics of Large Masses 1973 *Mesoscale meteorological phenomena*, UNESCO Summer School, Venice.

Nishioka, M. & Sato, H. 1974 Measurements of velocity distribution in the wake of a circular cylinder at low Reynolds Number. *J. Fluid Mech.* **65**, 97-112.

Pedlosky, J. 1979 *Geophysical fluid dynamics.* Berlin: Springer-Verlag.

Pitts, D. E., Lee, J. T., Fein, J., Sasaki, Y., Wagner, K. & Johnson, R. 1977 Mesoscale cloud features observed from Skylab. In *Skylab explores the Earth, NASA spec. Publs* **380**, 479-501.

Scorer, R. S. 1978 *Environmental aerodynamics.* Chichester: Ellis Harwood.

Takematsu, M. & Kita, T. 1978 Vortex shedding from Taylor columns. *J. Phys. Soc. Japan* **451**, 1781-1782.

Taneda, S. 1956 Experimental investigation of the wakes behind cylinders and plates at low Reynolds numbers. *J. Phys. Soc. Japan* **11**, 302-307.

Taneda, S., Honji, H. & Tatsuno, M. 1974 The behaviour of tracer particles in flow visualization by electrolysis of water. *J. Phys. Soc. Japan* **37**, 784–788.

Taneda, S., Honji, H. & Tatsuno, M. 1977 The electrolytic precipitation method of flow visualization. *Int. Symp. on Flow Visualization*. Tokyo, pp. 133–138.

Tritton, D. J. & Davies, P. A. 1981 Instabilities in geophysical fluid dynamics. In *Hydrodynamic instabilities and the transition to turbulence* (ed. H. L. Swinney & J. P. Gollub), pp. 229–270 (*Topics in applied physics*, vol. 45). Berlin: Springer-Verlag.

Tsuchiya, K. 1969 The clouds with the shape of Kármán vortex street in the wake of Cheju island, Korea. *J. met. Soc. Japan* **47**, 6, 457–465.

Vaziri, A. 1971 Rotating flow over shallow topographies. Ph.D. Dissertation, University of Delaware.

Vaziri, A. & Boyer, D. L. 1971 Rotating flow over shallow topographies. *J. Fluid Mech.* **50**, 79–95.

Vaziri, A. & Boyer, D. L. 1977 Topographically induced Rossby waves. *Archiv. Mech.* **29**, 3–12.

Vaziri, A. 1977 Topographic effects of rotating flows on a beta plane. *Recent Adv. Engng Sci.* **8**, 205–213. (Proc. 10th Anniv. Meeting Soc. Engng Sci.) Boston: Scientific Publishers.

Walker, J. D. A. & Stewartson, K. 1972 The flow past a circular cylinder in a rotating frame. *Z. angew. Math. Phys.* **23**, 745–752.

White, W. B. 1971 A Rossby wake due to an island in an eastward current. *J. phys. Oceanogr.* **1**, 161–168.